MICHIGAN STATE UNIVERSITY

CYCLOTRON LABORATORY

THE ϵ/β^+ DECAY OF ^{145}Gd: RESOLUTION OF ϵ/β^+ DECAY BRANCHING RATIO ANOMALIES AND EVIDENCE FOR PRONOUNCED STRUCTURES IN THE β-DECAY STRENGTH

R.B. FIRESTONE, R.C. PARDO, R.A. WARNER, Wm. C. McHARRIS, and W.H. KELLY

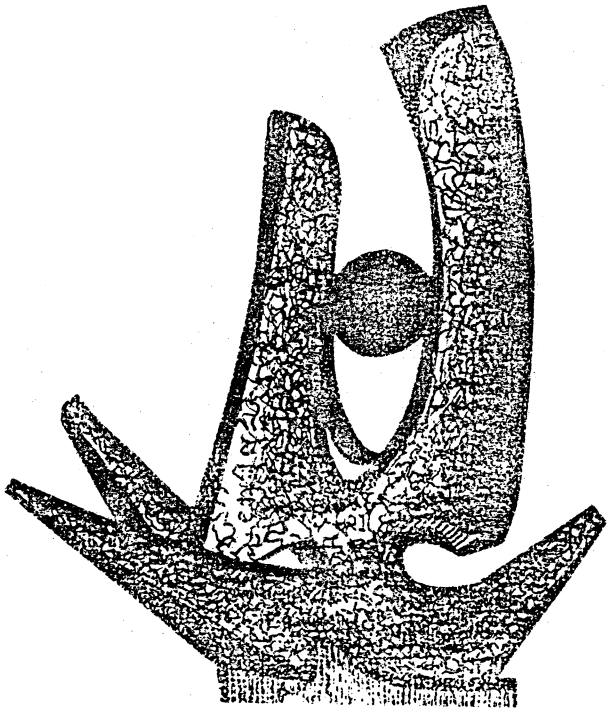

MARCH 1981

MSUCL-347

~~MSUNC-220~~

MSUCL-347
MSUNC-220

THE ϵ/β^+ DECAY OF ^{145}Gd: RESOLUTION OF ϵ/β^+ DECAY BRANCHING RATIO ANOMALIES AND EVIDENCE FOR PRONOUNCED STRUCTURES IN THE β-DECAY STRENGTH

R.B. Firestone,[a] R.C. Pardo,[b] R.A. Warner,[c] Wm. C. McHarris, and W.H. Kelly[d]

National Superconducting Cyclotron Laboratory and
Departments of Chemistry and Physics
Michigan State University
East Lansing, Michigan 48824

[a]Present Address: Nuclear Science Division, Lawrence Berkeley Laboratory, University of California, Berkeley, CA 94720.

[b]Present Address: Physics Division, Argonne National Laboratory, Argonne, IL 60439.

[c]Present Address: Battelle Northwest, 320 Bldg.-300 Area, P.O. Box 999, Richland, WA 99352.

[d]Present Address: Department of Physics and Office of the Dean, College of Letters and Science, Montana State University, Bozeman, MT 59717.

ABSTRACT

The ϵ/β^+ decay of 23.0 min ^{145}Gd has been thoroughly studied with Ge(Li) and plastic scintillator detectors. A total of 326 γ rays de-exciting 136 levels in ^{145}Eu have been placed by this work. The available decay energy, Q_ϵ=5.07±0.06 MeV, was measured by β-γ coincidence techniques. ϵ/β^+-decay branching ratios have been measured for several transitions, and a long standing anomaly in those ratios has been resolved by the new Q_ϵ value and the discovery of additional electron-capture decay. We have investigated the β-strength function for ^{145}Gd and discovered pronounced structure with resonances at 1042, 1819, 2484, and 4500 keV. The 1042-keV resonance is proposed to result from a $(\pi d_{3/2})^2(\nu s_{1/2})^{-1}\rightarrow(\pi d_{3/2})^1$ β-transition, the 1919- and 2584-keV resonances from $(\pi d_{5/2})^2\rightarrow[(\pi d_{5/2})\otimes 2^+]_1$, decays, and the very strong 4500-keV resonance from the $(\pi h_{11/2})^2\rightarrow(\pi h_{11/2})\otimes(\nu h_{9/2}+\nu f_{7/2}+\ldots)$ transition across the shell closure.

[RADIOACTIVITY ^{145}Gd; measured E_γ, γ-γ coin, E_β, β-γ coin, Q, $t_{1/2}$, x-γ coin, $\gamma^{\pm}$-γ coin; deduced ϵ/β^+ ratios, logft, β-strength function, missing continuum decay intensity. ^{145}Eu; deduced levels, J, π; calculated level energies with shell model, weak-coupling model.]

I. INTRODUCTION

Since $^{145}Gd^{g}$ was first characterized in 1959 by Grover[1] and later by Olkowsky et al.,[2] it has continued to spark considerable interest and controversy. This decay is uncharacteristic when compared with the lighter N=81 odd-A isotones. Despite having much greater available decay energy, ^{145}Gd (in this paper ^{145}Gd will be taken to mean $^{145}Gd^{g}$ unless stated otherwise) is more than twice as long-lived as ^{143}Sm and displays a completely different decay pattern.

In 1970 Newman et al.[3] reported spins and parities for a number of the low-lying states in the ^{145}Eu daughter determined by the $^{144}Sm(\tau,d)^{145}Eu$ reaction, and they also reported the analysis of a high-resolution Ge(Li) γ-ray spectrum associated with ^{145}Gd decay.

In 1971 Eppley, McHarris and Kelly[4] presented a more complete decay scheme for ^{145}Gd that explained many of its decay properties. They showed that the unique ^{145}Gd decay pattern resulted partly from the crossing of the $\nu s_{1/2}$ state below the $\nu d_{3/2}$ state to become the ground state in ^{145}Gd. This effectively blocked all simple allowed β transitions between available shell-model states and forced the decay to proceed primarily to high-lying states of more complex character.

Although Eppley, McHarris, and Kelly resolved one controversy, they opened up another, more perplexing question. In the course of their decay-scheme studies, they measured ϵ/β^{+}-decay branching ratios (hereafter referred to as ϵ/β^{+}) for the stronger β transitions from ^{145}Gd. Some of these values deviated significantly from allowed β-decay theory and could not be explained at that time. Firestone et al.[5,6] pursued this question in 1974-75 in a series of progressively more precise experiments; yet the

ϵ/β^{+} anomalies persisted. They proposed[7] that the inclusion of second-order corrections to the allowed theory of ϵ/β^{+} ratios might produce such anomalies in *hindered* allowed decays, but, as this suggestion could not be experimentally verified for the complex ^{145}Gd decay, the matter remained in question.

In 1976 Firestone et al.[8] reported a more complete Ge(Li) γ-ray singles spectrum for ^{145}Gd taken with a larger detector than had been previously available. In this spectrum numerous new γ-ray lines were observed above 2.5 MeV, representing about 4% of the total decay intensity. This unplaced intensity was insufficient by itself to remove the anomalies but pointed out possible difficulties with the accepted decay scheme. The next year Hornshøj, Nielsen, and Rud[9] (hereafter HNR) measured a ^{145}Gd γ-ray singles spectrum in which they reported that some 16% of the total γ-ray intensity existed in transitions above 2.5 MeV. In addition, they measured a new total decay energy by a questionable (see §III.C. below) γ-ray endpoint technique and obtained a Q_{ϵ} that was 320 keV lower than the previously accepted value and which could help remove the ϵ/β^{+} anomalies. Also, HNR concurred with an argument of Hardy et al.[10] that the decay of ^{145}Gd should proceed to a large density of states above 2.5 MeV in ^{145}Eu, which would deexcite by numerous, weak γ-ray transitions individually difficult to detect, yet containing a large total amount of decay intensity.

Our (Firestone et al.[8]) recent γ-ray singles intensities could not be reconciled with those of HNR, and their new decay energy was uncertain because it failed to correct both for Compton events and nuclear structure effects. Nevertheless, the basic argument of Hardy et al. offered a plausible explanation for the apparent ϵ/β^{+} anomalies. We therefore

decided to remeasure the ^{145}Gd decay scheme completely with sufficient precision to settle this matter finally. Despite the dire warning of HNR that this would be "quite out of the reach of current γ-spectroscopic techniques," we have successfully restudied the decay of ^{145}Gd and our results are detailed in this paper.

II. SOURCE PREPARATION

Sources of ^{145}Gd were prepared both by the ^{144}Sm(^{3}He,2n)^{145}Gd reaction using a 20-MeV ^{3}He beam and the ^{144}Sm(α,3n)^{145}Gd reaction using a 42-MeV α beam from the Michigan State University 50-MeV sector-focused cyclotron. Targets of $^{144}Sm_2O_3$ (enriched to >95% in ^{144}Sm and obtained from Oak Ridge National Laboratory) were bombarded in the various experimental configurations discussed below. Very pure sources of ^{145}Gd were produced in both reactions, because the lighter Gd products were all too long lived ($t_{1/2} \geq 36$ h) to contribute significantly to the activity at the time of counting. The bombardment energy was chosen to avoid the production of ^{144}Gd($t_{1/2}$=4.5 min). In addition, the sources were permitted to cool for about one half-life (23 min) in order to allow short-lived activities to die away. This removed impurities resulting from oxygen in the target as well as the decay of $^{145}Gd^{m}$ ($t_{1/2}$=85 sec), which was produced copiously in both reactions. The sources produced in these reactions were transported to the counting areas either by a fast rabbit system (transit time <10 sec) or by a He-jet recoil-transport system (HeJRT)[11] (transit time <1 sec). The latter system was automated so that sources could be collected, allowed to cool, and automatically moved in front of the detectors in a repeating cycle in order to maximize counting efficiency. Activity transported by the rabbit system was manually removed from the rabbit and allowed to cool before counting.

III. EXPERIMENTAL DATA

A. γ-Ray Singles Spectra

Two separate Ge(Li) detectors were used to record the ^{145}Gd γ-ray singles spectra. One detector with 2.0 keV resolution and 8% efficiency (relative to a 7.6×7.6-cm NaI (Tl) detector at 25 cm for 1333 keV) was used to record the spectra below 2.7 MeV. A second detector, with 2.1-keV resolution and 16% efficiency, was used to observe the higher energy γ rays. A pile-up rejection system was employed to minimize chance γ-ray summing, and all sources were counted at a distance of 50 cm at rates below 5000 cps to minimize coincident summing. The sources were enclosed in Be absorbers sufficiently thick to stop all positrons in order to reduce the background from bremsstrahlung.

Data were recorded in two consecutive 25-min spectra from an 8192-channel ADC, and the second spectrum was subtracted from the first, after being normalized to the long-lived impurity peaks. In this manner a total of 2×10^9 events, exclusive of annihilation radiation, were recorded on magnetic tape. The spectra were then calibrated up to 4.8 MeV for energy and intensity with the sources listed in Table I. These calibrations were performed with the configuration identical to that for the ^{145}Gd sources both before and after the experiments. Internal energy calibrations were also performed with live ^{145}Gd sources. The resulting spectra were then interactively analyzed using the computer code SAMPO[12] to obtain the best set of peak centroids and areas. The complexity of the spectrum required the stripping of numerous multiplets of γ rays, which was performed by requiring both a minimum standard deviation and a satisfactory visual acceptance of the fit.

In addition, the high energy of many of the γ rays further complicated the spectrum with the contribution of single- and double-escape peaks. In order to correct for these escape-peak intensities, the efficiency for detection of single- and double-escape peaks as a function of γ-ray energy was calibrated using ^{66}Ga and ^{56}Co sources. The resultant "escape efficiency curve" is shown in fig. 1. For γ rays below 2.5 MeV this correction becomes small. We found that for our detection system, the ratio of single- to-double escape-peak intensities remained constant at a value of 1.20 for all γ-ray energies. The escape peak intensity was then stripped from the spectrum before final analysis.

The γ-ray singles spectrum (uncorrected) is shown in fig. 2, and a list of the ^{145}Gd γ rays and their intensities is given in Table II.

B. Coincidence Spectra

Activity produced by the $^{144}Sm(\alpha,3n)^{145}Gd$ reaction was transported using the HeJRT System and deposited on a programmable, movable tape. These sources were deposited for 20 min, moved to a Pb shielded area for another 20 min to allow short-lived activity to die away, and then counted for 20 min. This permitted nearly continuous counting without manual intervention, allowing us to obtain a large number of coincidence events. The two Ge(Li) detectors discussed above were placed at about 135° with respect to the source in order to reduce the contributions from annihilation and Compton scattering to the spectrum. Standard fast-slow coincidence electronics were used, and γ-γ-t triplets were stored sequentially on magnetic tape. Timing resolution of $\tilde{\sim}$15 nsec fwhm was obtained during the course of the experiment, and both detectors were gated on γ rays up to 5.5 MeV. Over a period of three days we obtained 1.3×10^7 pairs of coincident events which were then analyzed. Over fifty gates were set on each side, and, in order to improve the statistics, the corresponding gates were precisely matched in gain, using a quadratic fit to the centroids of several intense peaks, and then they were summed. This procedure contributed negligible loss of resolution and allowed us to use all of the data most effectively.

The integral coincidence spectrum is displayed in fig. 3, and gates on the 330-, 808-, and 1042-keV γ rays deexciting the first three populated excited states of ^{145}Eu are shown in figs. 4-6. A summary of the coincidence information is included in Table II. It is important to note that sufficient statistics were obtained to see several transitions above 4.0 MeV quite clearly. In this region the background was very low, and only

a small number of events were actually necessary to determine a coincidence definitely. Whenever possible, the coincidence assignments were checked for intensity by comparison with the singles intensities; however, many γ rays could be observed unambiguously only in coincidence experiments. As in the singles spectrum, coincidences were corrected for single- and double-escape peaks.

C. Decay Energy

Three early measurements[1,2,13] of the β endpoint for ^{145}Gd decay yielded the decay energy, Q_ε = 5.31±0.12 MeV.[14] Although Wapstra[15] proposed a systematic value, Q_ε = 5.0 MeV, nine separate calculations tabulated by Maripuu[16] yielded a higher average value, Q_ε = 5.19±0.07 MeV, the error representing the statistical scatter of the calculations.

HNR suggested that the previous experimental Q_ε values were too high because they represented gross β endpoints and failed to account adequately for a weak, high energy β^+ branch, thereby giving too large a value. They then reported a new value, Q_ε = 5.00±0.07 MeV, measured by a different technique. They utilized their γ-ray singles spectrum by plotting the square-root of the number of events vs the γ-ray energy to obtain a γ-ray endpoint. This value was taken to represent the endpoint for *K* capture, assuming a statistical capture feeding to a continuum of states in ^{145}Eu.

We believe that this technique cannot be acceptable because of several severe deficiencies. An experimental Ge(Li) γ-ray spectrum is not simply a collection of γ-ray energies but is normally dominated by the Compton scattered events from the higher energy transitions. Thus, a γ-ray spectrum endpoint will tend to primarily be a Compton endpoint that at higher energies is about 0.24 MeV below the highest energy γ ray. In addition it is impossible to account for the clustering of γ-ray peak intensity, due to nuclear structure, as is observed in the ^{115}Cd singles spectrum near the γ-ray endpoint.

To demonstrate this more clearly we have repeated HNR's method with our own γ-ray singles spectrum. This result is shown in fig. 7, where the data are compressed and plotted in the same way as by HNR. Our endpoint, Q_ε = 4.86±0.03 MeV, is even lower than that of HNR and is not consistent with any previously measured or calculated value. In Table III we have presented the existing experimental endpoint values for Q_ε before our present work.

To obtain a more reliable value of Q_ε, we have performed standard β-γ coincidence experiments in order to label the various β^+ branches directly by their subsequent γ-ray deexcitations. Mixed sources of ^{145}Gd and internal β^+-calibration standards were prepared using the HeJRT system and transported to a point between the 16% Ge(Li) and a 5.1×5.1-cm Pilot B plastic scintillator detector. A 6.4-μm Mylar window separated the source in the evacuated tape transport box from the plastic detector. A standard fast-slow coincidence electronics system was used to record β-γ-*t* triplets on magnetic tape for off-line analysis. β-γ coincidence spectra were then recovered for the strong γ-ray transitions associated with ^{145}Gd decay and the standards. Only direct ground state γ-ray transitions were utilized in order to minimize coincident summing, and the mixed sources obviated the need for count-rate and source-thickness corrections. The β-γ coincidence spectra for the 1758- and 1881-keV γ rays of ^{145}Gd and the 378-keV γ ray of ^{53}Fe are shown in figs. 8-10.

A simple Fermi-Kurie plot cannot be used to analyze β^+ spectra taken with plastic scintillators because of backscattering, summing with annihilation radiation, and numerous other effects. We therefore analyzed our data using a method developed by Davids et al.[17] We fitted a smooth curve through a standard β^+ spectrum (here the 1758-keV gate) and numerically generated a standard experimental spectrum shape. Utilizing this standard shape, we normalized the other spectra to the same intensity and calculated a linear "stretch factor" that is proportional to the end-point width of the distribution. The resultant fits are drawn through the data in figs. 8-10. The stretch factors were assumed to vary linearly with

end-point energy over moderate ranges of energy.

The results of this analysis are shown in Table IV. The stretch factors we used were all nearly unity, justifying a linear interpolation; however, we have also fitted idealized β^+ spectra to estimate a correction for any small nonlinearities. We have now adopted the resultant value, Q_ε = 5.07±0.06 MeV, with a 2σ statistical error. This value is 0.2 MeV larger than that obtained by the use of HNR's technique and is in agreement with our suggestion of the dominance of Compton events in their method. Although most calculations were slightly higher than our final value, it agrees with the systematic estimate of Wapstra.[15]

D. Half-life

Although the ^{145}Gd half-life has been measured several times in the past, we have remeasured it again during these experiments. The previous values are presented in Table V. Sources of ^{145}Gd were prepared with the aid of the HeJRT system and counted for seven consecutive 10-min intervals with the 16% Ge(Li) detector. The count rate was kept below 2000 cps at all times, and sources were held for 20 min before counting in order to allow short-lived activities, particularly ^{145}Gd^m, to decay away. This latter point was critical because 85-sec ^{145}Gd^m decays primarily to ^{145}Gd^g, which would perturb a measured half-life.[18] A pulse generator was included for a dead-time correction that was, however, small. The half-life was followed for both the 1758- and 1881-keV γ rays, and in fig. 11 we show the resultant half-life plot. We obtained a half-life of 23.0 ±0.4 min, which compares favorably with the early values and falls between the more recent measurements of Eppley, McHarris, and Kelly[4] and of HNR.

E. ε/β^+-Decay Branching Ratios

Our initial motivation for studying ^{145}Gd decay, of course, was the elucidation of the ε/β^+-decay branching ratios. Since Eppley, McHarris, and Kelly[4] first measured apparently large anomalies in some of these ratios, we have performed a long series of complementary experiments designed to test their existence. It is interesting to note that Eppley, McHarris, and Kelly's early experimental results were essentially confirmed by our later, more precise measurements. We will show below that these data can now be reevaluated, with knowledge of the new decay scheme, to remove the evidence for large ε/β^+-branching anomalies.

1. *Pair Coincidence Spectra*. To obtain the relative β^+ feedings from ^{145}Gd decay, a $\gamma^\pm$-γ triple coincidence experiment was performed. Sources of ^{145}Gd were placed between Teflon absorbers of sufficient thickness to stop all emitted positrons. These sources were then placed in the center of a 20×20-cm NaI(Tℓ) split annulus.[19] The two optically isolated halves of the annulus were gated on the 511.0-keV $\gamma^\pm$ radiation marking a positron decay, and a third γ-ray coincidence was sought in the 16% Ge(Li) detector. The resulting $\gamma^\pm$-γ coincident spectrum is shown in fig. 12.

Although in principle the resulting spectrum represents only the ^{145}Gd β^+ decay, in fact several important corrections were necessary to obtain the proper transition intensities. The largest correction was for the summing of coincidence γ rays in the NaI(Tℓ) annulus. The high efficiency of the annulus (60% at 511 keV) led to significant coincidence summing and a resulting intensity loss for cascade γ rays. Whenever possible, direct ground-state transitions were chosen to obtain the relative level

feedings. The experimental data were analyzed to generate an appropriate sum intensity correction curve which was necessary in light of the new, more complex decay scheme. Fortunately, most of the new decay data resulted from electron capture decays, so these corrections were generally small. A second important correction was for annihilation in flight. Higher energy positrons are expected to annihilate in flight with greater probability and therefore will not emit so many 511-keV γ rays. We thus chose a low-Z absorber to mimimize this effect. The data were then corrected for annihilation in flight using the tables of Azuelos and Kitching.[20] This correction varied from about 2% at 1 MeV to 5% at 4 MeV.

2. *x-γ Coincidence Spectra*. Relative ε feedings were measured in an x-γ coincidence experiment. A 5-mm thick planar Ge(Li) detector having 550-eV resolution at 122 keV was used to gate on the *K* x-rays tagging an ε decay, and the 16% Ge(Li) detector was gated on γ rays labeling the ε-fed level (here internal conversion x-rays were always negligible). The data were written in three parameter x-γ-*t* event format on magnetic tape for off-line gating and analysis. The resultant γ-ray coincidence spectrum is shown in fig. 12. This spectrum was analyzed, with major corrections, to obtain the relative ε feedings. As with the positron coincidence data, it was necessary to correct for coincident summing, here in the x-ray detector. Although summing losses were less here (typically 20-30%), the preponderance of new decays were fed by ε decay, requiring important corrections. As before, the data themselves were utilized to generate the correction factors. A second correction peculiar to this experiment was for the higher-shell ε decay, which varies with the decay energy in a well known manner.[25] Additional information obtained from this experiment, resulting from the excellent timing of the planar Ge(Li) detector, was that all of the strong γ-ray transitions were essentially prompt ($t_{1/2}$ <0.5 nsec), justifying our use of the coincidence intensities. In fig. 13 we have shown the gated TAC spectra for several transitions.

3. *Absolute ε/β^+-Decay Ratios*. Although the x-γ and $\gamma^{\pm}$-γ experiments yielded relative ε- and β^+-feeding intensities, a third experiment was necessary to normalize the two sets of data. In this experiment thin sources of ^{145}Gd were prepared by deposition on Mylar tape from the nozzle of the HeJRT system. Annihilation radiation and K x-rays were counted simultaneously with a 7.6-cm×7.6-cm NaI(Tℓ) detector. The coincident γ rays, tagging the ε/β^+-fed levels in ^{145}Eu, were detected by the 16% Ge(Li) detector, and the source was surrounded by a lucite absorber to insure total β^+ annihilation. Coincident energies were recorded as γ-γ-t triplets on magnetic tape for off-line analysis. NaI(Tℓ) pulse-height spectra in coincidence with the γ rays depopulating the 808- and 1758-keV levels are shown in fig. 14. The relative efficiency ratio between the x-ray region (45 keV) and 511 keV was calibrated, using an NBS standard γ-ray source, as $R=\varepsilon(45)/\varepsilon(511)=2.00\pm0.14$. This compares favorably with $R=1.95$ that we calculated using the tabulated NaI(Tℓ) efficiencies of Heath[23] and correcting for attenuation by the source annihilator and detector windows with the tables of Israel.[24]

The ε/β^+ ratios were then determined absolutely for the strong transitions after additional corrections for the well-known fluorescence yields,[25] $\varepsilon(K)/\varepsilon(\text{tot})$ ratios,[25] and annihilation in flight.[20] The transitions to the 1042-, 1758-, and 1881- keV levels in ^{145}Eu were measured with sufficient precision to serve as primary absolute ε/β^+ ratio standards. Using the more extensive x-γ and β^+-γ coincidence data described above, we then calculated the absolute ε/β^+ ratios to other levels. These absolute values, including all corrections described above, are compared with the theoretical values,[26] assuming $Q_\varepsilon=5.07\pm0.06$ MeV, in Table VI. The skew ratio (exp/theory) is now nearly unity, within error, for all cases -- in agreement with allowed decay theory. We have also included in Table VI a comparison of the total ε/β^+-feeding intensities to each level inferred from the coincidence data (normalizing to the total singles intensity) with those obtained from γ-ray singles intensities through each level. The agreement is excellent, indicating that nearly all of the decay intensity has now been observed and that our corrections to the coincidence data are reasonable.

IV. PROPOSED DECAY SCHEME

Our proposed decay scheme for ^{145}Gd is shown in fig. 15. It is largely in agreement with the scheme of Eppley, McHarris, and Kelly[4] except for the level they previously reported at 953.4 keV, which has been deleted, and the addition of numerous new levels and γ-rays. We have now placed a total of 326 γ rays deexciting 136 levels in ^{145}Eu. A list of the levels placed in ^{145}Eu is given in Table VII. This is nearly an order of magnitude more levels and γ rays than were formerly observed by Eppley, McHarris, and Kelly, commensurate with our increase in statistics. Although complex decay schemes like ^{145}Gd cannot be entirely resolved experimentally, we believe that more than 98% of the total decay intensity is now placed. This is confirmed by the intensity balance through the two $7/2^+$ states at 330 and 1600 keV. A total of 53 γ rays, representing about 5% of the total intensity, feed these two states, which deexcite by only two strong γ rays. We observed that the ratio of the γ-ray intensity feeding to that deexciting these levels is 1.01±0.03, which is consistent with the expectation of no direct, second-forbidden ε/β^+ decay feeding to the levels. Any unobservable decay intensity would surely be reflected in this intensity balance. The level energies presented are unusually precise because they were fitted, using the numerous γ-ray relations, with the computer code GTOL[27] to obtain the best values.

We were able to assign the spin and parity of many states from a combination of deductions. The spin of the parent ^{145}Gd has been measured directly to be $1/2^+$.[28] Several low-lying states in ^{145}Eu were observed by Newman et al.[3] who made some J^π assignments using their data from ^{144}Sm(τ,d)^{144}Eu. Using their measurements we have assigned J^π's for

the states at 0 ($5/2^+$), 329.9 ($7/2^+$), 716.1 ($11/2^-$), 808.3 ($1/2^+$), 1041.7 ($3/2^+$), and 1600.3 ($7/2^+$) keV. In addition, numerous $3/2^+$ states can be assigned by their γ-ray decay patterns. Allowed and first forbidden nonunique decay from ^{145}Gd can only proceed to $1/2^\pm$ and $3/2^\pm$ states. If the states fed directly by ε/β^+ decay deexcite through known low-lying $7/2^+$ states, they are uniquely determined to be $3/2^+$. (Here we assume that all states that are fed with a $\log ft \leq 8.5$ and deexcite through a $7/2^+$ state are $3/2^+$.) A total of 45 states were assigned $3/2^+$ in this manner.

The relative γ-ray intensities listed in Table II are given as percent per decay. All transitions placed on the decay scheme evidenced at least weak coincidence information or were too strong not to have been observed in coincidence and thus were assumed to be direct ground-state transitions. The higher-energy γ rays had only limited possibilities for placement, making their assignments more straightforward. Energy sums were used only to assign a group of γ rays, already placed together in the scheme by coincidence information, to a given level. At high excitation in ^{145}Eu the level density is large enough to establish some question as to whether some levels are actually doublets or not. Although no satisfactory solution to this problem is apparent, this will not significantly effect the discussion below.

The level scheme, although quite complex, can be broken down into several dissimilar regions. Below 1.6 MeV only the 1042-keV state is fed measurably by ε/β^+ decay (≈8% of the total). The states at 1758 and 1881 keV are each fed by nearly 35% of the total ε/β^+ decay, and near 2.6 MeV three states receive 4.6% of the decay. In the region from 2.7 to 4.0 MeV many very weakly-fed states are observed, but above 4.0-MeV, ten states are seen to receive about 5% of the total decay. When one considers the

strong energy dependence of ϵ/β^+ decay, the total intensities to those high-lying states is indeed remarkable and indicative of an extremely non-statistical decay pattern.

V. DISCUSSION

With the completion of this complex and substantially more complete decay scheme than had previously existed for ^{145}Gd, the question of ϵ/β^+ anomalies can be answered with considerable certainty. Also, using one of the most detailed decay schemes yet studied for a nucleus far from stability, we can probe the nature of β decay to regions of high level density. ^{145}Eu is a particularly suitable choice for this study because it lies on the N=82 closed shell and is only one proton removed from the Z=64 semi-closed shell. The unusual decay properties of ^{145}Gd will be shown to be readily explained by use of the weak-coupling plus shell models.

A. ϵ/β^+ Ratios

The final ϵ/β^+ ratios obtained from this work are presented in Table VI. None of the strongly fed levels now shows any measurable anomaly. The weighted average skew ratio for all measured levels (experiment/theory) is 1.2±0.1, indicating less than a 30% deviation from theory. Small deviations have been observed experimentally before and are probably explained by higher order theoretical corrections.[29] No adequate explanations exist for large anomalies,[30] and our results now remove this likelihood for ^{145}Gd decay.

The apparent anomalies were removed by the inclusion of additional ε-decay intensity and a lower decay energy as was suggested by HNR. It is impossible to reconcile our γ-ray intensity above 2.5 MeV with that reported by HNR because we see only about one-third of their reported intensity, and such a large amount of missing decay would completely destroy the intensity balances through the lower-lying states. We did observe almost 10% of the decay to occur from new γ rays below 2.5 MeV, however, which was sufficient to support HNR's general argument. We also consider our general agreement with HNR on the β^+-decay endpoint to be strictly fortuitious. Their method was shown to be in error by our better statistics, confirming our claim that their result should be dominated by Compton events. Nevertheless, it must be emphasized that HNR were correct in suggesting that the endpoint should be lower for the strongest ϵ/β^+ transitions to agree with theory.

B. Statistical β-Decay Properties

The large amount of decay data discussed here offers a unique opportunity to investigate the nature of β decay to regions of high level density. Although individual transitions in this region cannot be fruitfully discussed, previous authors have differed in their statistical treatment of such decay systematics. Duke et al.[31] have presented NaI(Tℓ) γ-ray spectra that they interpreted to indicate slowly varying β-decay strengths (corrected for energy dependence) to regions of high level density for a broad range of nuclei in the region $182 \leq A \leq 210$. A similar argument was given by Hardy et al.,[10] who present a simulated, computer-generated, decay scheme argument with the same conclusion. Finally, Kratz et al.,[32,33] using β-delayed neutron decay data, have suggested that strong shell-model structure is observed in the β-decay strength function near Z=50. All of these discussions offer incomplete or inferred evidence for their claims. We believe that our data can be much more clearly interpreted in investigating the β decay of ^{145}Gd to high-lying states in ^{145}Eu.

The work of Hardy et al.[10] is particularly relevant to this discussion because they created a simulated γ-ray spectrum for ^{145}Gd (dysphemistically called "Pandemonium"). Briefly, they manufactured a decay scheme assuming the level density formulas of Gilbert and Cameron, level separations according to the Wigner law, a random Porter-Thomas distribution of β-decay transition probabilities, and constant β strengths.[34] In addition, they assumed that all $3/2^+$ states deexcite to the ground and all $1/2^+$ states deexcite to a level at 800 keV. A "γ-ray spectrum" was thus generated corresponding to various "experimental" statistical degrees of precision. It was asserted that ≈1000 γ rays should be present and that for a spectrum with the statistical precision presented by Eppley, McHarris, and Kelly,[4]

≈20% of the decay would not have been observed. Further, it was asserted that additional γ rays from the deexcitation of the levels to various additional states would further disperse the total γ-ray intensity.

The data presented in this paper invalidate some of the assumptions of Hardy et al. concerning Pandemonium. The $3/2^+$ states tend not to deexcite strongly to the ground state but instead spend most of their γ ray intensity to numerous excited states up to 3 MeV in ^{145}Eu. The other higher-lying states of unknown spin (largely $1/2^+$ states) are also seen to spread their intensity to many excited states, although generally they feed the ground state more strongly than the 808-keV state. This deexcitation pattern is completely alien to that assumed by Hardy et al. Also, according to their analysis, we should have seen only about 80 of the ≈1000 γ rays expected to have energies greater than 1.7 MeV. In fact, we observed ≈200 γ rays in this energy region (albeit some only in coincidence experiments). Indeed, the ≈1000 γ-ray estimate is very misleading because most such transitions, even though they might exist, are much too weak to be of any consequence to the level scheme. (Certainly all γ-ray transitions between all levels are possible with finite transition probability. Nevertheless, only those transitions with appreciable intensity need be considered in constructing a level scheme. In this sense no decay scheme can ever be considered really complete but is only an asymptotic approximation; yet it is only in the driest academic sense that such arguments should be considered important.) For the 136 levels presented here, ≈9000 γ rays are possible, so we only see some 3.5% of the numerical total. This has been shown to represent more than 98% of the total γ-ray intensity.

Finally, the assumption by Hardy et al. of a constant β-decay strength can be tested with our data. The β-decay strength function is normally

defined as

$$\overline{S}_{\beta}(E) = \frac{b(E)}{ft} \text{ MeV}^{-1}\text{sec}^{-1},$$

which effectively removes the statistical factor energy dependence. Here $b(E)$ is the transition intensity per MeV and ft is the normal β-decay transition rate. We have plotted our ^{145}Gd β-strength function in fig. 16. The data are averaged in 200-keV intervals of excitation to remove small experimental and statistical fluctuations. The large peak in the β-decay strength at 1.8 MeV is acknowledged by Hardy et al. to be structure related, and the second, weak peak at 2.6 MeV generally agrees with their prediction of "broad topographical features" in the β-strength function. The large peak at 4.5 MeV, however, completely disagrees with the structureless β-strength function arguments. Clearly, the decay of ^{145}Gd, after correction for the known energy dependence in the decay rate, proceeds substantially to pronounced structure comprised of some 25 constituent levels near 4.5 MeV. This fact cannot be removed by such experimental problems as the uncertainty in the decay energy or the unresolved level doublets, because the absolute decay intensity is much larger to these states than to all other lower lying states above 2.7 MeV.

The previous work of Duke et al.[31] did not describe such structure; however, their data suffered from a combination of poor resolution and substantial corrections for detector response which could well have hidden strong, narrow structures in their measured β-decay strength functions. They also looked at different nuclei, which might or might not exhibit the same structure observed here. They did, however, see a large average β-strength increase at N=126.

It appears here that the suggestions of structure effects observed by Kratz et al.[32,33] near Z=50 may also be observed with more certainty

for ^{145}Gd decay. A more detailed explanation of what occurs for ^{145}Gd decay will be presented in the following section.

C. Weak-Coupling Plus Shell-Model Description of ^{145}Gd Decay

Although the ϵ/β^+ decay of an odd-A nucleus one nucleon removed from the N=82 closed and Z=64 semi-closed shells might appear easily explainable by the simple shell model, this is not the case for ^{145}Gd decay. A stylized diagram of the available shell model decay channels is shown in fig. 17. The ϵ/β^+ decay is effectively blocked, in a shell-model sense, because the available filled proton orbitals, $g_{7/2}$ and $d_{5/2}$, cannot decay directly to the open $s_{1/2}$ neutron hole in an otherwise closed neutron shell. Single-particle shell-model transitions cannot occur except by inclusion of $(\pi d_{3/2})^2$ or $(\pi s_{1/2})^2$ pairs in the proton wave functions.

The occupancy of $(\pi s_{1/2})^2$ orbitals must be small because they provide much less pairing energy than $(\pi d_{5/2})^2$ orbitals. This is demonstrated by the high $\log ft \geq 7.7$ for β decay to the $(1/2^+)$ 808-keV state in ^{145}Eu. The $(\pi d_{3/2})^2$ orbital does not suffer from so large a pairing energy deficiency; however, the $\pi d_{3/2} \rightarrow \nu s_{1/2}$ ϵ/β^+ transition will be ℓ forbidden. This explains the $\log ft$ of 6.7 for decay to the $(3/2^+)$ 1041.9-keV state in ^{145}Eu. An admixture of $(\pi h_{11/2})^2$ pairs to the proton wave function should be important because of the large pairing energy associated with high-ℓ orbitals; nevertheless, the $\pi h_{11/2} \rightarrow \nu s_{1/2}$ transition is highly forbidden and does not contribute to this discussion. Most of the ϵ/β^+ decay of ^{145}Gd is thus observed to proceed to more complex states than can be explained within the context of the simple shell model. We have chosen to explain the decay to states below 3 MeV in terms of transitions between collective core structures with the additional odd particles acting merely as spectators. We will also show that the strong decay intensity beginning near 4 MeV results from the opening of the next neutron shell and the resultant reappearance of simple shell-model type transitions.

For this discussion we have simplified our complex decay scheme to include only the prominent structures observed in the β-strength function plotted in fig. 16 where resonances at 1043, 1819, 2584, and 4500 keV are featured. These resonances, in general, contain many individual substates (much like some resonances observed in particle-reaction data) and are assumed to have simple underlying structures. The energies given here represent the weighted average energy of all levels within the resonance. Our simplified decay scheme is shown in fig. 18a, and in fig. 18b we show the relevant core decay,[35] ^{144}Eu$\rightarrow^{144}$Sm, on which we shall base our weak-coupling model. The appropriate choice of a core is not obvious, as ^{146}Tb$\rightarrow^{146}$Gd might also be appropriate. Unfortunately, that decay has to our knowledge not yet been well enough investigated to be usable, so it will not be considered here.

1. *The 1819- and 2584-keV Resonances.* Most of the ϵ/β^+-decay strength (exclusive of the fast $\pi d_{5/2} \rightarrow \nu d_{3/2}$ single-particle ground-state transition) from ^{144}Eu goes to the lowest lying two 0^+ and 2^+ states in ^{144}Sm. The ground state of ^{145}Eu can be represented as a $\pi d_{5/2}$ single particle, and it is reasonable that decay should proceed to weakly-coupled states of the form, ^{144}Sm + $(\pi d_{5/2})$.

Although many possible low-lying couplings exist, only those which form $1/2^+$ or $3/2^+$ states in the odd-mass system can be observed from the allowed ϵ/β^+ decay. Therefore, the strong transitions from ^{144}Eu to the 0^+ states in ^{144}Sm cannot be observed in the odd-mass system because only a $5/2^+$ coupling is possible. The analog of the decay to the first two 2^+ states can be observed in the odd-mass system because there the $1/2^+$ and $3/2^+$ couplings are possible. We thus propose that the two resonances at

1819 and 2554 keV represent the $\pi d_{5/2} \otimes 2_1^+$ and $\pi d_{5/2} \otimes 2_2^+$ configurations. Each of these resonances consists predominantly of two distinct, ϵ/β^+-fed levels. One member of each pair of levels is definitely $3/2^+$ and the other is most likely spin $1/2^+$ (no γ-ray deexcitation is observed to the $\pi g_{7/2}$ level) as we would expect. A further check of our assignment is possible if we compare the relative γ transition intensities between the states of the odd- and even-mass systems. For the core decay (^{144}Eu) only a small γ-ray branch (4%) exists between the two 2^+ states, the remainder going to the ground state. The identical branching ratio is observed in the odd-mass system, with 96% of the decay again going to the ground state.

The excitation energies of the states in the odd- and even-mass systems are also quite similar. The states in the odd-mass system are about 160 keV higher, which may be explained by the residual interaction in that system. This is apparent because the two odd-mass excited resonances have almost exactly the same energy displacement (765 keV) as was observed in the even-mass system (763 keV). Such a result is expected if the residual interaction were the same for both states. For the $\pi d_{5/2} \otimes 2_1^+$ resonance it is possible to infer the location of the remaining $5/2^+$, $7/2^+$, and $9/2^+$ couplings, which are not fed directly by ϵ/β^+ decay. The two states at 1567.3 and 1599.9 keV are probably not populated appreciably by ϵ/β^+ decay but instead are strongly fed by γ-ray cascades. We thus propose that these states represent the $5/2^+$ and $7/2^+$ couplings, respectively. The remaining $9/2^+$ coupling may lie at 1459.6 keV. This state is only very weakly populated because only ($5/2^+$) states populated by forbidden β decay can deexcite to it. The centroid energy of these five couplings is 1653 keV, which agrees closely with the energy of the 2_1^+

state (1660 keV), as would be expected in our weak coupling model.

Finally, if our decay model is correct, the logft's observed in the even-mass system should coincide with those in the odd-mass system. Here it appears that the ^{144}Eu β decays are considerably faster. On closer inspection, however, the large decay energy for ^{144}Eu (Q_ϵ=6.33 MeV) should tell us that much decay intensity was not observed for the same reasons as in the early ^{145}Gd decay studies. If, instead, we take the logft's from the better studied ^{142}Pm decay[36] (Q_ϵ=4.89 MeV) we get logft= 5.3 and 6.2 for the decays to the 2_1^+ and 2_2^+ states respectively. Again the agreement with the odd-mass decay is striking. Thus, our simple weak-coupling model can be used to explain in detail much of the decay systematics to the lower-lying states.

2. *The 4500-keV Resonance*. The simple weak-coupling model which successfully explained decay to the lower-lying states in ^{145}Eu cannot be so easily applied to the states that form the large upper resonance. Beginning at 4.05 MeV we observe 21 states having β decay with logft's $\lesssim$6.5. No other β transitions so fast are observed to any other states above 2.7 MeV. The rapid decline in β strength following the peak at 4.5 MeV can only be observed up to about 4.8 MeV. Even fast transitions to levels above this energy will have too little decay intensity to be observed as discreet transitions. Nevertheless, the continuum γ-ray intensity falls off rapidly in this region (above the highest-energy Compton-scattering events). Clearly a simple structure, favored for population by ε/β^+ decay, must occur at 4.5 MeV in ^{145}Eu.

As discussed above, there is possibly a significant admixture of $(\pi h_{11/2})^2$ pairs in the proton wave function of ^{145}Gd. Simple $\pi h_{11/2}\rightarrow\nu h_{9/2}$ spin-flip transitions will be very fast. Thus if the shell separation energies in this region are small enough, these β transitions should be observed. In addition, the $\pi h_{11/2}$ orbitals can decay by an ℓ-forbidden allowed transition to the $\nu f_{7/2}$ level. We can thus explain the decay systematics to the large resonance as resulting from the opening of the next shell and subsequent fast transitions to three-quasiparticle configurations of the form, $[\pi h_{11/2}\otimes\nu h_{9/2}\otimes(\nu s_{1/2}+\nu d_{3/2})]$.

In order to estimate the excitation energy of the $\nu h_{9/2}$ and $\nu f_{7/2}$ orbitals in ^{145}Eu, we have performed a simple shell-model calculation, the results of which are shown in fig. 19. Here the $\nu h_{9/2}$-$\nu h_{11/2}$ separation is taken as 5.5 MeV, the pairing energy from mass-excess data[15,37] is 1.72 MeV, and the empirical shell-model pairing interaction $V_{9/2\text{-}11/2}$ is 1.25 MeV.[38] The lower-lying single-particle neutron energies are obtained

from the ^{145}Eu data and the N>82 neutron single-particle energies are taken from the level scheme of ^{147}Gd.[39] Although the $\nu h_{9/2}$ orbital lies 1 MeV too high for the expected resonance, additional residual interactions in the three-quasiparticle structures can further lower the energies of the low-spin couplings. Also, we find that the $\nu f_{7/2}$ orbital lies at 3.9 MeV, where the large β-strength resonance begins. Direct $\pi h_{11/2}\rightarrow\nu f_{7/2}$ transitions are ℓ-forbidden and will not alone produce a strong β-decay resonance; however, configurations such as $[(\nu h_{11/2}\otimes\nu f_{7/2})\otimes(\nu s_{1/2}\otimes\nu d_{3/2}^{+}\ldots)]$ will certainly mix strongly with the $\nu h_{9/2}$ coupled states, thus lowering the energy of some states expected to be strongly populated by ε decay. We thus suggest that it is probable that the strong β feeding centered at 4.5 MeV in ^{145}Eu results primarily from the $\nu h_{11/2}\rightarrow\nu h_{9/2}$ transition. The strength of this transition can be predicted by comparison with the same transition observed in the ε/β^+ decay of the $\pi h_{11/2}$ isomer of ^{147}Tb ($t_{1/2}$=1.9 min)[39] to the $\nu h_{9/2}$ state in ^{147}Gd. A logft of 4.3 was observed there, which compares favorably with the logft of 4.8 that we measured for decay to the 4.5-MeV resonance. This comparison is enhanced by the fact that the high decay energy for ^{147}Tb (Q_ε=6.3 MeV) indicates that missing γ-ray intensity should substantially increase that logft, while for ^{145}Gd only a portion of the $\nu h_{9/2}$ strength can be observed, thereby lowering the true logft for that transition.

VI. CONCLUSIONS

From this detailed investigation of the decay of ^{145}Gd, >98% of the ε/β^+-decay intensity has been placed. This information has been sufficient to answer some perplexing problems concerning the decay. Previously measured large anomalies in the experimental ε/β^+ decay branching ratios have been shown to disappear as a result of our new measurement of the Q_ε value and the discovery of numerous, weaker-ε-fed levels at high excitations in ^{145}Eu. The systematics of the ε/β^+-decay to 136 levels in ^{145}Eu have been described using simple models which are outlined in fig. 19. Transitions to the lower-lying single-particle states were shown to be highly retarded because of a severe mismatch in the proton-neutron shell-model wave functions. Substantial decay was observed to proceed to two resonances at 1819 and 2584 keV. These resonances could be readily described in a weak-coupling model as the $\pi d_{5/2}\otimes(2_1^+ + 2_2^+)$ states arising from the coupling of the odd valence proton to the 2^+ ^{144}Sm core states. Finally, a substantial β-strength resonance at 4.5 MeV was shown to represent decay from $(\pi h_{11/2})^2$ quasipairs to $(\nu h_{9/2}+\nu h_{7/2})$ states across the shell gap, thus populating $[\pi h_{11/2}\otimes(\nu h_{9/2}+\nu g_{7/2})\otimes(\nu s_{1/2}+\nu d_{3/2})]$ three-quasiparticle configurations in ^{145}Eu.

Although we have achieved considerable success in explaining the nature of ^{145}Gd decay, several interesting experiments still remain to test our ideas. The decay of ^{145}Gd^m offers an excellent opportunity to test our explanation for the 4.5 MeV resonance. Here the high-spin three-quasiparticle states of the form, $[\pi h_{11/2}\otimes(\nu h_{9/2}+\nu h_{7/2}+\ldots)\otimes\nu h_{11/2}]_{9/2^-,11/2^-,13/2^-}$ should be populated. Although experimental difficulties resulting from contamination from the ^{145}Gd^g decay cannot be avoided here, the additional

0.75 MeV of decay energy may well allow observation of the resonance at higher excitations. Also, the study of ^{147}Dy decay (Q_ε=6.3 MeV) should present opportunity to observe the same resonance, but with sufficient β-decay energy to populate it throughout its extent. In addition, work is in progress to reinvestigate existing decay schemes for similar structure in β-decay strengths. Preliminary results for ^{143}Sm and ^{141}Nd decays indicate substantial evidence for the $\pi d_{5/2}\otimes[2_1^+ + 2_2^+]$ resonances, although decay across the shell gap is not possible in those cases. Similar structures are also seen away from the shell closure, at lower energies, consistent with increasing deformation. We shall investigate these phenomena in future publications.

ACKNOWLEDGEMENTS

We thank the staff of the National Superconducting Cyclotron Laboratory of Michigan State University for their considerable assistance in performing these experiments. We also thank the Michigan State University nuclear chemistry and physics students for their help in collecting data. The Isotopes Project at Lawrence Berkeley Laboratory is also thanked for the use of the decay scheme analysis and production programs, as well as their aid in preparation of this manuscript. Finally, we especially thank Dr. G.F. Bertsch and Dr. R.G.H. Robertson for their helpful discussions concerning the conclusions presented in this paper.

This work was supported in part by the U.S. National Science Foundation under Grant No. PHY76-04912. Partial support for one of the authors (RBF) was provided by the U.S. Department of Energy under Contract W-7405-ENG-48.

References

[1]J. R. Grover, Phys. Rev. 116, 406 (1959).

[2]J. Olkowsky, M. Le Pape, I. Gratot, and L. Cohen, J. Phys. Radium 20, 549 (1959).

[3]E. Newman, K. S. Toth, R. L. Auble, R. M. Gaedke, M. F. Roche, and B. H. Wildenthal, Phys. Rev. C 1, 1118 (1970).

[4]R. E. Eppley, Wm. C. McHarris, and W. H. Kelly, Phys. Rev. C 3, 282 (1971).

[5]R. B. Firestone, R. A. Warner, Wm. C. McHarris, and W. H. Kelly, Phys. Rev. Lett. 33, 30 (1974).

[6]R. B. Firestone, R. A. Warner, Wm. C. McHarris, and W. H. Kelly, Phys. Rev. Lett. 35, 401 (1975).

[7]R. B. Firestone, R. A. Warner, Wm. C. McHarris, and W. H. Kelly, Phys. Rev. Lett. 35, 713 (1975).

[8]R. B. Firestone, R. A. Warner, Wm. C. McHarris, and W. H. Kelly, Annual Report of the Michigan State University Cyclotron Laboratory 1974-76, E. Lansing, Mich., pp. 71-72.

[9]P. Hornshøj, H. L. Nielsen, N. Rud, Phys. Rev. Lett. 39, 537 (1977).

[10]J. C. Hardy, L. C. Carraz, B. Jonson, and P. G. Hansen, Phys. Lett. 71B, 307 (1977).

[11]K. L. Kosanke, M. D. Edmiston, R. A. Warner, R. B. Firestone, Wm. C. McHarris, and W. H. Kelly, Nucl. Instr. Meth. 120, 199 (1974).

[12]J. T. Routti and S. G. Prussin, Nucl. Instr. Meth. 72, 125 (1969). We used a variant of this program adapted for interactive use on the NSCL PDP 11/45 computer by C. B. Morgan.

[13]R. Arlt, G. Beyer, G. Musiol, L. K. Peker, G. Pfrepper, and H. Strusmy, Izv. Akad. Nauk SSSR, Ser. Fiz. 34, 409 (1970).

[14]This value was adopted in T. W. Burrows, Nucl. Data Sheets 12, 203 (1974).

[15]A. H. Wapstra and K. Box, At. Data and Nucl. Data Tables 19, 215 (1977).

[16]1975 Mass Predictions, S. Maripuu editor, At. Data and Nucl. Data Tables 17, pp. 533-535 (1976).

[17]For a description of this technique see, for example, C. N. Davids, D. R. Goosman, D. E. Alburger, A. Gallman, G. Guillaume, D. H. Wilkinson, and W. A. Lanford, Phys. Rev. C 9, 216 (1974).

[18]R. E. Eppley, Wm. C. McHarris, and W. H. Kelly, Phys. Rev. C 2, 1929 (1970).

[19]W. H. Kelly and Wm. C. McHarris, International Conference on Radioactivity in Nuclear Spectroscopy, Vanderbilt University, 11-15 August 1969, Proceedings, Vol. II (contributed papers), p. 1435 (1972), Gordon and Breach, New York.

[20]G. Azuelos and J. E. Kitching, At. Data and Nucl. Data Tables 17, 103 (1976).

[21]A. H. Wapstra, G. J. Nijgh, and R. Van Lieshout, Nuclear Spectroscopy Tables, North-Holland Publishing Co., Amsterdam, 1959.

[22]This standard consists of ^{57}Co, ^{60}Co, ^{85}Sr, ^{88}Y, ^{109}Cd, ^{113}Sn, $^{113}In^{m}$, ^{137}Cs, $^{137}Ba^{m}$, ^{139}Ce, and ^{203}Hg, deposited as the chlorides and sulfides on 0.006-cm thick polyester tape and covered by another layer of the same tape. This point source was calibrated by the National Bureau of Standards for absolute efficiency to better than 3% at all energies.

[23]R. L. Heath, Scintillation Spectrometry Gamma-Ray Spectrum Catalogue, U. S. Atomic Energy Commission Research and Development Report No. IDO-16880-1, 1964 (unpublished), Vol. 1.

[24]I. Israel, Nucl. Data, Sect. A 7, 565 (1970).

[25]W. Bambynek, B. Craseman, R. W. Fink, H.-U. Freund, H. Mark, C. D. Swift, R. E. Price, and P. V. Rao, Rev. Mod. Phys. 44, 716 (1972).

[26]N. B. Gove and M. J. Martin, Nucl. Data, Sect. A 10, 205 (1971).

[27]W. B. Ewbank, computer code GTOL (Nuclear Data Project, Oak Ridge National Laboratory). Modified by B. J. Barton and J. K. Tuli (National Nuclear Data Center, Brookhaven National Laboratory). For a discussion of this code see Brookhaven National Laboratory Report BNL-NCS-23375, pp. 1-5 (1977).

[28]C. Ekström, S. Ingleman, M. Olsmats, and B. Wannberg, Phys. Scr. 6, 181 (1972).

[29]R. B. Firestone, Wm. C. McHarris, and B. R. Holstein, Phys. Rev. C 18, 2719 (1978).

[30]W. B. McFarland and W. W. Repko, Phys. Rev. C 15, 809 (1977).

[31]C. L. Duke, P. G. Hansen, O. B. Nielsen, G. Rudstam, and the Isolde Collaboration, CERN, Nucl. Phys. A 151, 609 (1970).

[32]K. L. Kratz, W. Rudolph, H. Ohm, H. Franz, M. Zendel, G. Herrmann, S. G. Prussin, F. M. Nuh, A. A. Shihab-Eldin, D. R. Slaughter, W. Halverson, and H. V. Klapdor, Nucl. Phys. A 317, 335 (1979).

[33]K. L. Kratz, H. Ohm, K. Summerer, M. Zendel, G. Jung, K. D. Wunsch, C. Ristori, J. Crancon, and S. G. Prussin, Phys. Lett. 86, B 21, (1979).

[34]The procedure is discussed in detail by B. Jonson, B. Hayberg, P. G. Hansen, P. Hornshøj, and P. Tiedemand-Peterson, Third International Conference on Nuclei Far from Stability, Cargese, Corsica, 19-26 May 1976, Proceedings, CERN Report 76-13, p. 277.

[35]G. G. Kennedy, S. C. Gujrathi, and S. K. Mark, Z. Phys. A 276, 103 (1976).

[36]S. Raman, J. L. Foster, O. Dietzsch, D. Spalding, L. Bimbot, and B. H. Wildenthal, Nucl. Phys. A 201, 21 (1973).

[37]R. C. Pardo, S. Gales, R. M. Ronningen, and L. H. Harwood, Phys. Lett. 91B, 41 (1980).

[38]G. F. Bertsch, The Practitioner's Shell Model, American Elsevier Publishing Co., New York, 1972; also private communication.

[39]E. Newman, K. S. Toth, D. C. Hensley, and W.-D. Schmidt-Ott, Phys. Rev. C 9, 674 (1974); 12, 346(E) (1975).

Table I

Energy and Intensity Calibration Standards for ^{145}Gd γ-Ray Spectra

^{22}Na	^{75}Se	^{207}Bi
^{56}Co	^{94}Nb	^{226}Ra
^{60}Co	^{152}Eu	^{228}Th
^{66}Ga	^{166}Ho^{m}	

Table II

γ Rays Observed From ^{145}Gd Decay

E_γ (keV)	I_γ [a]	Placement from-to (keV)	Observed in Coincidence Gate(s) (keV)
287.2(20)	0.007(1)	2049-1761	953
305.5(30)	0.007(2)	2417-2114	1784
310.1(30)	0.011(2)	2422-2114	1784
329.9(1)	2.7 (2)	330-0	1436,1719,1784,1873, 2195
514.0(20)	0.007(2)	2114-1600	(1600)
589.0(20)	0.015(3)	2049-1460	1460
646.0(20)	0.019(4)	2562-1915	1915
716.2(2)	0.071(6)	1758-1042	1042
719.9(1)	0.105(10)	1761-1042	1042
722.0(20)	0.020(6)	2322-1600	(1600)
751.0(20)	0.015(3)	2319-1567	1567
754.6(2)	0.034(6)	2322-1567	1567
808.4(1)	8.6 (5)	808-0	950,953,1072,1891, 2150,2292,2423,2867
818.0(20)	0.120(13)	2700-1881	1881
838.8(1)	0.30 (2)	1881-1042	1042
854.1(20)	0.034(5)	2422-1567	1567
933.7(20)	0.013(3)	2780-1845	1845
949.7(1)	0.68 (4)	1758-808	808
952.6(3)	1.50 (9)	1761-808	808,2423
961.0(20)	0.032(5)	2562-1600	(1600)
973.8(20)	0.010(4)	2819-1845	1845
984.0(20)	0.032(5)	2586-1600	(1600)
992.5(20)	0.010(4)	2839-1845	1845

Table II (continued)

E_γ(keV)	I_γ[a]	Placement from-to (keV)	Observed in Coincidence Gate(s) (keV)
1013.9(20)	0.010(3)	2859-1845	1845
1014.2(2)	0.071(6)	2780-1766	1436
1041.8(1)	9.9 (6)	1042-0	839,1422,1600,3010
1072.3(1)	2.8 (2)	1881-808	808
1082.4(20)	0.029(5)	2839-1758	1758
1129.8(1)	0.024(3)	1460-330	330
1181.5(1)	0.074(13)	3062-1881	1881
1215.0(20)	0.046(7)	2972-1758	1758
1220.3(20)	0.016(4)	2028-808	808
1234.4(20)	0.041(7)	2043-808	808
1366.1(20)	0.082(11)	3769-2402	808,(1594)
1380.1(1)	0.07 (2)	2188-808	808
1381.0(20)	0.054(8)	2422-1042	1042
1416.3(20)	0.008(4)	3880-2463	1422
1421.7(1)	0.042(6)	2463-1042	1042
1427.9(20)	0.12 (3)	1758-330	330
1430.8(4)	0.061(12)	1761-330	330
1436.2(2)	0.30 (2)	1766-330	330
1441.5(20)	0.016(7)	3769-2327	2327
1459.6(3)	0.081(9)	1460-0	
1461.6(1)	0.28 (2)	3062-1600	1600
1462.9(20)	0.025(5)	3229-1766	1436
1466.6(20)	0.029(8)	3547-2079	2079
1467.6(20)	0.007(3)	3932-2463	1422
1513.2(20)	0.017(5)	3628-2114	1784
1513.4(2)	0.35 (2)	2322-808	808
1561.9(20)	0.014(6)	3889-2327	2327

Table II (continued)

E_γ(keV)	I_γ[a]	Placement from-to (keV)	Observed in Coincidence Gate(s) (keV)
1567.2(1)	0.97 (6)	1567-0	
1576.0(20)	0.025(6)	3176-1600	1600
1576.0(20)	0.019(6)	4276-2700	1891
1593.8(1)	0.176(11)	2402-808	808
1598.6(20)	0.095(11)	2642-1042	1042
1599.0(20)	0.039(10)	3199-1600	1600
1600.1(1)	1.76 (10)	1600-0	1460,2150,2947
1613.9(1)	0.130(11)	2422-808	808
1620.3(1)	0.10 (6)	3221-1600	1600
1648.9(20)	0.024(8)	3705-2054	2054
1658.0(1)	0.38 (2)	2700-1042	1042
1678.6(2)	0.052(8)	2487-808	808
1686.6(1)	0.105(12)	2495-808	808
1696.4(2)	0.043(7)	2504-808	808
1719.1(2)	1.05 (7)	2049-330	330
1750.1(20)	0.033(5)	2079-330	(330)
1755.0(20)	0.046(11)	4282-2525	2195
1757.9(1)	34.2 (20)	1758-0	2739
1782.9(20)	0.036(10)	4309-2525	2195
1784.4(1)	0.40 (3)	2114-330	330
1788.5(20)	0.075(10)	4710-2919	808
1796.1(20)	0.007(3)	3562-1766	1436
1844.0(20)	0.007(3)	4309-2463	(1042),2463
1845.4(1)	0.53 (4)	1845-0	
1858.3(20)	0.10 (2)	3739-1881	1881
1872.6(20)	0.109(11)	2203-330	330
1880.6(1)	32.6 (19)	1881-0	
1891.0(2)	0.43 (3)	2700-808	808

Table II (continued)

E_γ(keV	I_γ [a]	Placement from-to (keV)	Observed in Coincidence Gate(s) (keV)
1915.5(2)	0.19 (2)	1915-0	
1934.8(20)	0.048(9)	2743-808	(808)
1988.5(1)	0.090(10)	2319-330	330
1999.0(20)	0.057(5)	4048-2049	330,1719
2021.7(20)	0.105(8)	3062-1042	1042
2027.8(1)	0.148(11)	2029-0	
2040.9(20)	0.07 (2)	3921-1881	1881
2042.9(1)	0.049(10)	2043-0	
2049.1(4)	0.15 (2)	2049-0	
2054.1(1)	0.080(11)	2054-0	
2056.7(20)	0.08 (2)	2940-1881	1881
2064.0(20)	0.09 (2)	3945-1881	1881
2073.9(20)	0.018(7)	3921-1845	1845
2077.9(20)	0.066(14)	4282-2203	2203
2079.1(1)	0.11 (2)	2079-0	
2083.7(1)	0.099(8)	4547-2463	1042,1422
2083.9(20)	0.027(7)	3963-1881	1881
2087.2(20)	0.076(14)	3848-1761	953
2091.4(2)	0.049(10)	4410-2319	(330,2319)
2100.4(1)	0.205(13)	4503-2402	808
2110.6(1)	0.138(13)	2919-808	808
2144.2(3)	0.037(5)	4259-2114	(1784)
2149.0(20)	0.070(15)	3747-1600	(1600)
2149.6(1)	0.130(9)	2150-0	
2157.9(20)	0.032(4)	2487-330	330
2158.6(20)	0.022(7)	4004-1845	1845
2163.4(1)	0.119(12)	2972-808	808

Table II (continued)

E_γ(keV)	I_γ [a]	Placement from-to (keV)	Observed in Coincidence Gate(s) (keV)
2175.8(20)	0.032(10)	4700-2525	2195
2181.2(1)	0.105(9)	4503-2322	(2322)
2187.8(3)	0.018(8)	2188-0	2203
2192.0(20)	0.034(8)	3001-808	(808)
2195.2(2)	0.099(10)	2525-330	330
2202.0(20)	0.063(15)	4282-2079	2079
2203.0(20)	0.052(13)	4391-2188	2188
2203.4(1)	0.45 (3)	2203-0	
2227.0(1)	0.140(13)	4276-2049	330,1719
2232.6(2)	0.035(10)	2562-330	330
2239.7(3)	0.016(7)	3281-1042	1042
2253.9(2)	0.078(9)	3062-808	808
2276.1(6)	0.006(2)	4391-2114	(1784)
2283.5(3)	0.026(3)	4044-1761	808,953
2292.0(4)	0.05 (3)	3101-808	808
2293.5(2)	0.10 (3)	4052-1761	808,953
2302.0(20)	0.015(5)	4184-1881	1881
2313.0(20)	0.056(8)	2642-330	(330)
2318.9(1)	0.052(4)	2319-0	
2322.0(4)	0.118(14)	2322-0	
2327.3(7)	0.04 (2)	2327-0	
2349.0(1)	0.050(6)	2349-0	
2360.9(4)	0.022(5)	4410-2049	(330,1719)
2387.3(2)	0.054(13)	4436-2049	(330),1719
2390.9(2)	0.032(8)	3199-808	808
2396.5(4)	0.035(6)	4276-1881	1881
2409.9(20)	0.018(5)	3452-1042	1042
2413.3(2)	0.34 (2)	4259-1845	1845
2416.8(1)	0.33 (2)	2417-0	

Table II (continued)

E_γ(keV)	I_γ [a]	Placement from-to (keV)	Observed in Coincidence Gate(s) (keV)
2422.9(1)	0.074(8)	4184-1761	808,953
2425.6(1)	0.192(13)	4184-1758	1758
2429.6(1)	0.091(8)	3238-808	808
2451.9(2)	0.15 (3)	4052-1600	1600
2453.0(20)	0.019(6)	4503-2049	(330),1719
2458.9(1)	0.035(5)	3267-808	808
2463.3(8)	0.042(6)	2463-0	
2469.6(1)	0.080(13)	4070-1600	1600
2487.8(3)	0.036(7)	2487-0	
2494.8(1)	1.33 (8)	2495-0	
2504.3(1)	0.099(7)	2504-0	
2508.0(20)	0.023(7)	4391-1881	1881
2509.2(20)	0.018(7)	4276-1766	1436
2521.5(20)	0.04 (2)	4282-1758	1758
2539.0(20)	0.010(5)	4309-1766	1436
2544.9(7)	0.054(9)	2545-0	
2554.8(7)	0.061(12)	4436-1881	1881
2562.7(7)	0.043(7)	2562-0	
2573.9(1)	0.102(8)	4454-1881	1881
2585.7(1)	0.33 (2)	2586-0	
2589.2(2)	0.048(13)	3398-808	808
2591.3(20)	0.006(3)	4473-1881	1881
2597.3(2)	0.039(4)	4646-2049	(330,1719)
2603.2(2)	0.052(11)	3412-808	808
2606.1(2)	0.127(9)	2606-0	
2609.6(2)	0.051(8)	4454-1845	1845
2622.1(1)	0.052(11)	4503-1881	1881

Table II (continued)

E_γ(keV)	I_γ [a]	Placement from-to (keV)	Observed in Coincidence Gate(s) (keV)
2624.7(2)	0.017(6)	4391-1766	(330,1436)
2633.1(20)	0.033(4)	3676-1042	1042
2642.2(1)	2.09 (12)	2642-0	
2662.7(2)	0.062(9)	4424-1761	(808,953)
2670.0(20)	0.039(9)	4428-1758	1758
2670.7(2)	0.066(6)	4432-1761	808,953
2675.2(3)	0.064(10)	4276-1600	1600
2677.9(2)	0.085(10)	4436-1758	1758
2691.0(9)	0.021(4)	4259-1567	1567
2697.2(9)	0.08 (2)	4454-1758	1758
2700.9(9)	0.021(4)	2700-0	
2708.5(1)	0.064(6)	4309-1600	1600
2714.4(5)	0.079(6)	4282-1567	1567
2738.7(1)	0.068(5)	4497-1758	1758
2742.7(1)	0.114(7)	2743-0	
2754.1(1)	0.043(3)	3754-0	
2764.8(1)	0.072(5)	4646-1881	1881
2779.9(1)	0.041(5)	2780-0	
2789.5(2)	0.069(8)	4547-1758	1758
2797.4(2)	0.037(6)	4555-1758	1758
2800.7(2)	0.039(10)	4566-1766	330,1436
2804.9(2)	0.062(9)	4566-1761	808,953
2809.9(2)	0.034(6)	4410-1600	1600
2819.8(2)	0.021(2)	3628-808	(808)
2828.2(1)	0.087(6)	4428-1600	1600
2831.0(20)	0.024(8)	4710-1881	1881
2836.0(2)	0.20 (2)	4436-1600	1600

Table II (continued)

E_γ(keV)	I_γ[a]	Placement from-to (keV)	Observed in Coincidence Gate(s) (keV)
2838.7(1)	0.34 (2)	2839-0	
2842.9(2)	0.060(5)	4410-1567	1567
2853.2(2)	0.048(5)	4454-1600	1600
2860.9(2)	0.027(4)	4428-1567	1567
2867.4(2)	0.084(8)	3676-808	808
2884.1(2)	0.109(9)	4646-1761	808,953
2887.9(6)	0.045(4)	4646-1758	1758
2896.9(2)	0.083(5)	3705-808	808
2902.3(2)	0.029(3)	4664-1761	808,953
2907.2(7)	0.035(8)	3950-1042	1042
2918.6(2)	0.052(4)	2919-0	
2947.1(3)	0.098(10)	4547-1600	1600
2947.2(20)	0.064(9)	3989-1042	1042
2955.4(2)	0.041(9)	4555-1600	1600
2971.9(4)	0.021(5)	2972-0	
2980.1(3)	0.028(7)	4547-1567	(1567)
2988.1(4)	0.023(3)	2988-0	
2992.9(3)	0.026(6)	4593-1600	(1600)
3001.5(2)	0.055(6)	3001-0	
3009.7(2)	0.051(5)	4052-1042	(1042)
3034.0(3)	0.028(3)	4635-1600	1600
3039.5(2)	0.059(9)	3848-808	808
3053.0(20)	0.18 (3)	3383-330	330
3063.1(2)	0.068(5)	3062-0	
3079.0(2)	0.041(3)	3409-330	330
3092.0(2)	0.219(13)	3092-0	
3101.2(2)	0.160(10)	3101-0	

Table II (continued)

E_γ(keV)	I_γ[a]	Placement from-to (keV)	Observed in Coincidence Gate(s) (keV)
3114.2(2)	0.051(4)	3444-330	330
3141.3(7)	0.031(3)	3950-808	(808)
3176.3(2)	0.054(5)	3176-0	
3177.4(20)	0.07 (2)	3507-330	(330)
3188.0(20)	0.08 (2)	3520-330	(330)
3198.3(4)	0.017(3)	3199-0	
3217.2(6)	0.014(2)	4259-1042	(1042)
3220.7(3)	0.035(2)	3221-0	
3239.4(7)	0.027(4)	3238-0	
3243.2(7)	0.019(3)	4052-808	(808)
3253.6(3)	0.027(3)	3254-0	
3261.1(2)	0.094(6)	3261-0	
3266.0(20)	0.12 (2)	3267-0	
3280.7(2)	0.053(5)	3281-0	
3290.4(4)	0.015(4)	3620-330	330
3299.2(4)	0.007(3)	3628-330	330
3312.5(2)	0.051(4)	3312-0	
3324.9(20)	0.006(2)	4131-808	808
3343.5(3)	0.048(4)	3343-0	
3348.4(3)	0.023(3)	4157-808	808
3376.9(7)	0.023(5)	4184-808	808
3389.1(4)	0.022(4)	3389-0	
3394.5(3)	0.018(2)	4436-1042	1042
3408.3(20)	0.023(3)	3409-0	
3413.1(3)	0.059(3)	4454-1042	1042
3454.3(3)	0.015(5)	4497-1042	1042
3460.9(3)	0.069(8)	4503-1042	1042

Table II (continued)

E_γ(keV)	I_γ[a]	Placement from-to (keV)	Observed in Coincidence Gate(s) (keV)
3473.9(5)	0.179(10)	4282-808	808
3505.3(4)	0.031(4)	4547-1042	1042
3512.8(3)	0.054(10)	4555-1042	1042
3520.9(7)	0.009(1)	3520-0	
3525.6(7)	0.010(1)	3526-0	
3547.4(5)	0.025(4)	3547-0	
3550.7(3)	0.057(5)	4593-1042	1042
3556.5(3)	0.017(4)	4365-808	(808)
3578.4(4)	0.013(2)	3578-0	
3582.9(3)	0.041(3)	4391-808	808
3598.6(3)	0.026(3)	3599-0	
3601.5(3)	0.051(4)	4410-808	808
3604.2(3)	0.141(9)	4646-1042	
3619.8(7)	0.030(3)	3620-0	
3623.1(7)	0.010(4)	4664-1042	1042
3626.2(9)	0.025(3)	4436-808	808
3632.7(3)	0.015(2)	3963-330	330
3643.8(3)	0.064(8)	3644-0	
3645.8(3)	0.076(6)	4454-808	808
3656.2(7)	0.004(2)	4464-808	808
3664.1(4)	0.013(2)	4473-808	808
3684.3(3)	0.117(8)	4014-330	330
3687.7(3)	0.135(9)	4497-808	808
3694.3(3)	0.046(4)	4503-808	808
3705.8(3)	0.032(2)	3705-0	
3738.7(3)	0.024(2)	4537-808	(808)
3746.9(3)	0.035(8)	3747-0	

Table II (continued)

E_γ(keV)	I_γ[a]	Placement from-to (keV)	Observed in Coincidence Gate(s) (keV)
3757.7(4)	0.009(1)	4566-808	808
3769.0(4)	0.016(5)	3769-0	
3785.4(6)	0.014(2)	4593-808	808
3801.3(3)	0.077(7)	4131-330	330
3826.8(4)	0.009(2)	4635-808	(808)
3848.0(4)	0.010(1)	3848-0	
3888.8(4)	0.022(3)	3889-0	
3891.7(4)	0.019(3)	4700-808	808
3901.7(4)	0.028(3)	4710-808	808
3920.8(5)	0.009(2)	3921-0	
3928.8(4)	0.049(3)	4259-330	330
3931.8(6)	0.007(2)	3932-0	
3940.2(7)	0.007(2)	3940-0	
3950.7(7)	0.009(2)	3950-0	
3953.3(20)	0.015(3)	4282-330	330
3962.9(5)	0.021(4)	3963-0	
3977.9(5)	0.041(5)	4309-330	330
4012.3(9)	0.007(1)	4014-0	
4021.5(4)	0.033(3)	4022-0	
4023.8(9)	0.023(3)	4024-0	
4043.8(4)	0.024(4)	4044-0	
4051.2(9)	0.013(2)	4052-0	
4068.9(6)	0.015(2)	4070-0	
4081.2(4)	0.027(3)	4410-330	(330)
4107.0(5)	0.008(1)	4436-330	(330)
4155.0(15)	0.006(1)	4157-0	
4184.6(4)	0.022(2)	4184-0	
4188.2(4)	0.025(3)	4518-330	330

Table II (continued)

E_γ(keV)	I_γ [a]	Placement from-to (keV)	Observed in Coincidence Gate(s) (keV)
4217.2(4)	0.013(2)	4537-330	330
4258.4(9)	0.037(4)	4259-0	
4275.9(9)	0.082(9)	4276-0	
4281.7(9)	0.070(7)	4282-0	
4307.3(4)	0.078(5)	4309-0	
4316.3(4)	0.041(3)	4646-330	330
4364.5(5)	0.031(2)	4365-0	
4370.7(6)	0.006(1)	4700-330	(330)
4379.9(7)	0.012(2)	4710-330	330
4390.7(5)	0.022(2)	4391-0	
4409.8(5)	0.033(2)	4410-0	
4427.8(5)	0.013(1)	4428-0	
4453.8(7)	0.027(4)	4454-0	
4463.1(6)	0.002(1)	4464-0	
4473.3(5)	0.007(1)	4473-0	
4502.6(6)	0.032(5)	4503-0	
4517.5(5)	0.008(1)	4518-0	
4536.8(5)	0.019(2)	4537-0	
4547.1(5)	0.015(1)	4547-0	
4554.5(6)	0.017(1)	4555-0	
4566.6(5)	0.019(2)	4566-0	
4577.8(9)	0.004(1)	4578-0	
4593.4(6)	0.004(1)	4593-0	
4634.9(9)	0.005(1)	4635-0	
4645.7(5)	0.046(3)	4646-0	
4656.2(9)	0.008(1)	4656-0	
4663.8(9)	0.005(1)	4664-0	
4685.3(6)	0.008(1)	4685-0	
4699.6(9)	0.002(1)	4700-0	

[a] Intensity per 100 γ rays.

Table III

^{145}Gd Q_ε Measurements

		E_{β^+} (keV)	Q_ε (keV)
A.	Gross β Endpoints		
1.	Grover (1959)	2400±200	--
2.	Olkowsky et al. (1959)	2500±150	--
3.	Arlt et al. (1970)	2500±200	5300±200
	Adopted (NDS12-2)	2470±100	5311±120
		Endpoint	Q_ε
B.	γ-Ray Singles Endpoint		
1.	Hornshøj et al.	4950±70	5000±70
2.	This work	4858±30	?
C.	β-γ Coincidence		
	This work	Q_ε = 5070±60 keV (2σ)	

Table IV

^{145}Gd β Endpoint by β-γ Coincidences

Decay	E_γ (keV)	Stretch Factor	E_{β^+} (keV)	Q_ε (keV)
^{53}Fe→ ^{53}Mn	378	1.0175(60)	2343.2±0.2	--
^{60}Cu→ ^{60}Ni	3124	0.8534(186)	1982.7±1.8	--
^{60}Cu→ ^{60}Ni	3194	0.7940(100)	1912.7±1.8	--
^{145}Gd→^{145}Eu	1758	1.0000	2305 ±18	5085±18
^{145}Gd→^{145}Eu	1881	0.9467(44)	2195 ±32	5098±32

^{145}Gd Q_ε Uncorrected	5088±16
Theoretical Fermi Correction	- 22±13
Corrected value	5066±29 keV
Adopted value	5070±60 keV (2σ)

Table V

Summary of ^{145}Gd Half-Life Measurements

Reference	$t_{1/2}$(min)
1. Keller et al. (1968)	22.9(1)
2. Arlt et al. (1970)	23 (1)
3. Eppley et al. (1971)	21.8(6)
4. Hornshøj et al. (1978)	23.9(1)
5. This work	23.0(4)

Table VI

Absolute ε/β^+-Decay Branching Ratios for ^{145}Gd Decay

Level in ^{145}Eu (keV)	ε/β^+ Ratio		Skew Ratio (exp/theory)	Total %β Feedings	
	Experiment	Calculated[a]		Coincidence[c]	Singles
808.3	b	0.56(3)	b	2.0(10)	<1.1
1041.7	0.91(14)	0.71(4)	1.3(3)	7.3(5)	8.1 (6)
1567.1	<143	1.26(9)	<113	0.8(3)	0.67(7)
1600.3	b	1.31(10)	b	0.4(3)	0.05(15)
1758.0	1.93(20)	1.62(13)	1.2(2)	35.2(22)	34.3 (20)
1761.3	2.9 (13)	1.62(14)	1.8(10)	1.2(4)	1.25(10)
1845.3	<191	1.82(15)	<105	0.2(2)	<0.11
1880.6	2.14(20)	1.92(15)	1.1(2)	32.6(18)	34.8 (20)
2048.8	3.8 (19)	2.47(25)	1.5(9)	0.9(3)	0.89(8)
2114.3	13 (6)	2.75(27)	5 (3)	0.7(2)	0.33(4)
2494.9	5.2 (14)	5.4 (7)	1.0(4)	1.3(2)	1.43(8)
2642.2	8.0 (18)	7.6 (12)	1.1(4)	2.3(4)	2.24(12)

[a] N.B. Gove and M.J. Martin, Nucl. Data Tables 10, 205(1971). Calculated for Q_ε = 5.07(6) MeV.

[b] Indeterminate from the data. No significant direct β feeding remains after correction for feeding from the higher-lying states.

[c] Inferred from the coincidence intensity balances and normalized to the total decay intensity from γ-ray singles.

Table VII

Levels Observed in ^{145}Gd Decay

Level Energy (keV)[a]	Feeding[b]	J^π	logft
0.0		$5/2^+$	
329.92(7)		$7/2^+$	
808.33(5)	<1.1	$1/2^+$	>7.7
1041.71(6)	8.1 (6)	$3/2^+$	6.74(5)
1459.7 (1)	<0.1		8.5
1567.12(7)	0.067(7)		8.56(3)
1600.26(6)		$(7/2^+)$	
1758.03(6)	34.3 (20)	$3/2^+$	5.76(4)
1761.32(8)	1.25 (10)	$3/2^+$	7.20(5)
1765.8 (1)	<0.02		>9.0
1845.32(9)	<0.11	$(3/2^+)$	>8.2
1880.62(5)	34.8 (20)		5.70(4)
1915.5 (2)	0.17 (2)		7.99(6)
2027.8 (1)	0.164(12)		7.95(5)
2042.9 (1)	0.090(13)		8.20(7)
2048.8 (1)	0.89 (8)	$3/2^+$	7.21(5)
2054.1 (1)	0.056(14)		8.4 (1)
2079.1 (1)	0.05 (3)		8.4 (3)
2114.3 (1)	0.33 (4)	$3/2^+$	7.60(6)
2149.6 (1)	0.130(9)		7.99(5)
2188.4 (1)	0.04 (3)		8.5 (4)
2203.4 (1)	0.49 (4)	$3/2^+$	7.39(5)
2318.68(8)	0.108(15)	$(3/2^+)$	7.99(7)
2321.72(7)	0.42 (3)	$(3/2^+)$	7.40(5)
2327.3 (6)	<0.032		>8.5
2349.0 (1)	0.050(6)		8.31(6)

Table VII (continued)

Level Energy (keV)[a]	Feeding[b]	J^π	logft
2402.25(9)			
2416.8 (1)	0.338(21)		7.45(4)
2422.3 (1)	0.230(15)		7.61(5)
2463.5 (1)			
2487.2 (2)	0.120(12)	$3/2^+$	7.86(6)
2494.88(8)	1.43 (8)		6.78(4)
2504.41(9)	0.142(10)		7.78(5)
2525.2 (2)			
2544.9 (7)	0.054(9)		8.18(8)
2562.5 (2)	0.129(14)	$3/2^+$	7.79(6)
2585.7 (1)	0.362(21)	$(3/2^+)$	7.34(4)
2606.1 (2)	0.127(9)		7.78(5)
2642.2 (1)	2.24 (12)	$(3/2^+)$	6.52(4)
2699.7 (1)	0.93 (4)		6.87(4)
2742.7 (1)	0.162(12)		7.61(5)
2754.1 (1)	0.043(3)		8.18(5)
2779.9 (1)	0.125(9)		7.70(5)
2819.1 (1)	0.010(4)		8.8 (2)
2838.7 (1)	0.379(21)		7.19(4)
2859.2 (1)	0.010(3)		8.8 (1)
2918.9 (1)	0.115(17)		7.67(8)
2971.8 (1)	0.186(15)		7.44(5)
2988.1 (4)	0.023(3)		8.34(7)
3001.5 (2)	0.089(10)		7.74(6)
3062.14(8)	0.60 (3)	$(3/2^+)$	6.88(4)
3092.0 (2)	0.219(13)		7.31(4)
3101.1 (2)	0.21 (4)		7.32(9)
3176.3 (2)	0.079(8)	$(3/2^+)$	7.71(6)

Table VII (continued)

Level Energy (keV)[a]	Feeding[b]	J^π	logft
3199.1 (2)	0.088(14)	$(3/2^+)$	7.65(8)
3220.6 (1)	0.13 (6)	$(3/2^+)$	7.5 (2)
3228.7 (10)	0.025(5)		8.2 (1)
3238.0 (1)	0.118(9)		7.50(5)
3253.6 (3)	0.027(3)		8.13(6)
3261.1 (2)	0.094(6)		7.59(5)
3267.2 (1)	0.155(21)		7.37(7)
3280.9 (2)	0.069(9)		7.71(7)
3312.5 (2)	0.051(4)		7.82(5)
3343.5 (3)	0.048(4)		7.83(5)
3383.0 (10)	0.18 (3)	$3/2^+$	7.24(8)
3389.1 (4)	0.022(4)		8.15(9)
3397.6 (2)	0.048(13)		7.8 (1)
3408.9 (2)	0.064(5)	$3/2^+$	7.67(5)
3411.6 (2)	0.052(11)		7.8 (1)
3444.2 (2)	0.051(4)	$3/2^+$	7.75(5)
3451.6 (10)	0.018(5)		8.2 (1)
3507.4 (10)	0.07 (2)	$3/2^+$	7.6 (1)
3520.0 (6)	0.089(20)	$(3/2^+)$	7.5 (1)
3525.6 (7)	0.010(1)		8.41(6)
3547.1 (5)	0.054(9)		7.67(9)
3561.9 (10)	0.007(3)		8.6 (2)
3578.4 (4)	0.013(2)		8.27(8)
3598.6 (3)	0.026(3)		7.95(7)
3620.2 (4)	0.045(5)	$3/2^+$	7.70(7)
3628.3 (2)	0.045(7)	$3/2^+$	7.70(8)
3643.8 (3)	0.064(8)		7.53(7)
3675.7 (2)	0.117(9)		7.25(6)

Table VII (continued)

Level Energy (keV)[a]	Feeding[b]	J^{π}	logft
3705.4 (2)	0.139(10)		7.16(6)
3738.9 (10)	0.10 (2)		7.3 (1)
3747.2 (3)	0.105(17)	$(3/2^+)$	7.25(9)
3768.9 (4)	0.114(14)		7.20(7)
3847.9 (2)	0.145(17)		7.04(7)
3879.8 (10)	0.008(4)		8.3 (2)
3888.9 (4)	0.036(7)		7.6 (1)
3920.7 (4)	0.097(22)		7.2 (1)
3931.7 (6)	0.014(3)		8.0 (1)
3939.3 (6)	0.087(20)		7.2 (1)
3944.6 (10)	0.09 (2)		7.2 (1)
3949.8 (4)	0.075(9)		7.25(8)
3962.9 (5)	0.063(9)	$3/2^+$	7.31(8)
3988.9 (10)	0.064(9)		7.28(8)
4003.9 (10)	0.022(7)		7.7 (2)
4014.1 (3)	0.124(8)	$3/2^+$	6.98(6)
4021.6 (4)	0.033(3)		7.54(7)
4023.9 (9)	0.023(3)		7.70(8)
4044.5 (3)	0.050(5)		7.34(7)
4047.9 (10)	0.057(5)		7.28(7)
4051.7 (1)	0.33 (5)	$(3/2^+)$	6.52(9)
4069.9 (1)	0.095(14)	$(3/2^+)$	7.04(9)
4131.4 (3)	0.083(8)	$3/2^+$	7.04(8)
4156.7 (3)	0.029(4)		7.48(9)
4183.98(9)	0.326(17)		6.40(7)
4258.6 (2)	0.498(22)	$3/2^+$	6.13(8)
4275.9 (1)	0.358(22)	$(3/2^+)$	6.26(8)
4281.8 (3)	0.56 (4)	$3/2^+$	6.05(8)

Table VII (continued)

Level Energy (keV)[a]	Feeding[b]	J^{π}	logft
4308.6 (1)	0.236(15)	$3/2^+$	6.40(8)
4364.8 (3)	0.048(5)		7.0 (1)
4390.7 (2)	0.161(17)		6.5 (1)
4410.1 (1)	0.276(15)	$3/2^+$	6.2 (1)
4424.0 (3)	0.062(9)		6.8 (2)
4428.3 (1)	0.166(11)	$(3/2^+)$	6.4 (1)
4432.0 (3)	0.066(6)		6.8 (2)
4436.1 (1)	0.452(19)	$3/2^+$	5.9 (1)
4454.44(9)	0.443(25)	$(3/2^+)$	5.9 (1)
4463.8 (5)	0.006(2)		7.8 (2)
4472.8 (3)	0.026(4)		7.1 (1)
4496.6 (1)	0.218(12)		6.2 (1)
4502.77(8)	0.528(23)		5.8 (1)
4517.9 (4)	0.033(4)	$3/2^+$	7.0 (1)
4536.9 (5)	0.019(2)		7.2 (1)
4547.2 (1)	0.377(18)	$3/2^+$	5.9 (1)
4555.4 (1)	0.149(15)	$(3/2^+)$	6.2 (1)
4566.4 (1)	0.129(14)		6.3 (1)
4577.9 (9)	0.004(1)		7.8 (2)
4593.0 (2)	0.101(9)	$(3/2^+)$	6.3 (1)
4634.6 (2)	0.042(4)	$(3/2^+)$	6.6 (2)
4645.63(9)	0.493(16)	$3/2^+$	5.5 (1)
4656.3 (9)	0.008 (1)		7.3 (2)
4663.8 (2)	0.044(5)		6.5 (2)
4685.4 (6)	0.008(1)		7.2 (2)
4700.3 (3)	0.059(11)	$3/2^+$	6.3 (2)
4709.9 (4)	0.139(14)	$3/2^+$	5.9 (2)

[a] Level Energies fit by computer code GTOL, Ref. 27.

[b] Feedings given in percent per decay of ^{145}Gd.

FIGURE CAPTIONS

Fig. 1 Ratio of γ-ray peak intensity to total escape-peak intensity plotted as a function of γ-ray energy using transitions from ^{56}Co and ^{66}Ga decays. The intensity ratio of single-to-double-escape peaks was observed to remain constant at a value of 1.20 throughout the energy range covered here.

Fig. 2 Summed γ-ray singles of spectrum taken with 8% and 16% Ge(Li) detectors. Because of the complexity of the spectrum, only a few representative transitions are labeled. Below 2.7 MeV the data are plotted logarithmically and above that energy, linearly.

Fig. 3 Background subtracted, summed integral coincidence spectrum taken with 8% and 16% Ge(Li) detectors at ≈135°.

Fig. 4 Background subtracted, summed coincidence spectrum gated on the 330-keV γ-ray transition.

Fig. 5 Background subtracted, summed coincidence spectrum gated on the 808-keV γ-ray transition.

Fig. 6 Background subtracted, summed coincidence spectrum gated on the 1042-keV γ-ray transition.

Fig. 7 Square root of the total number of events in the γ-ray singles spectrum as a function of energy deposited in the detector. The errors below 4.8 MeV are contained within the points. Data significantly outside the line represent true nuclear structure in the spectrum. The error in the endpoint represents only the internal statistical fluctuations of the fit. We note that this endpoint is 0.2 MeV lower than was obtained in the β-γ coincidence experiment. This is consistent with the domination of the technique by Compton scattered events. Needless to say, this result should not be considered as a measurement but, instead, as a demonstration of an inherently flawed technique.

Fig. 8 Background subtracted β^+ spectrum, recorded with a Pilot B plastic scintillator, in coincidence with 1758-keV γ rays. This spectrum was used as the standard shape (fitted curve) for calibration of the data. The sharp peak at low energies represents the 511-keV Compton edge.

Fig. 9 Background subtracted β^+ spectrum in coincidence with the 1881-keV γ rays. The curve through the points represents the stretched fit of the 1758-keV standard spectrum to this data.

Fig. 10 Background subtracted β^+ spectrum in coincidence with 2343-keV γ rays from the ^{53}Fe standard source. The curve through the points represents the stretched fit of the 1758-keV standard spectrum to this data.

Fig. 11 Plot of half-life data for ^{145}Gd summed over the 1758- and 1881-keV transition intensities. The half-life and error result from a least-squares-fit to the data.

Fig. 12 Background subtracted coincidence spectra utilized to obtain relative β^+-feedings ($\gamma^{\pm}$-γ) and relative ε-feedings (x-γ).

Fig. 13 TAC spectra coincident with the more intense γ rays from ^{145}Gd decay. The integral TAC is <15 nsec fwhm. The abscissa scale is roughly 1 nsec per channel.

Fig. 14 Background subtracted coincidence spectra, taken with a 7.6×7.6 cm NaI(Tℓ) detector, of x-rays and annihilation radiation in coincidence with the 808- and 1758-keV γ rays. The measured efficiency ratio $\varepsilon(45)/\varepsilon(511)=2.00\pm0.14$, was utilized with this data to generate the absolute normalization of the relative ε- and β^+-feeding shown in fig. 12. Note that after correction for γ-ray feeding from above, no significant β^+-feeding to the 808-keV level remains.

Fig. 15 Level scheme for the decay of 23.0-min ^{145}Gd. Transitions were placed on the basis of coincidence assignments (dotted if uncertain) as described in Table VII. The γ-ray intensities are given in percent per decay and logft values are calculated assuming $Q_\varepsilon=5.07\pm0.06$ MeV. Spin assignments are based on the (τ,d) reaction of Ref. 3, and all levels populated with log$ft\leq8.5$ which deexcite through the $7/2^+$ 330-keV or $(7/2^+)$ 1600-keV states are assigned $3/2^+$ and $(3/2^+)$, respectively.

Fig. 16 The β-strength function $\overline{S}(\beta)$ (per 200 keV) plotted as a function of excitation energy in ^{145}Eu. Here we define $\overline{S}(\beta)=b(E)/ft$ where $b(E)$ is the intensity fraction per 200-keV interval of excitation and ft is the standard β decay rate to that energy domain of the daughter. Broad resonances at 1.8-, 2.6-, and 4.5-MeV are observed, and the effective logft's to these resonances are shown.

Fig. 17 Stylized drawing of the available shell-model space, including virtual proton pairs, for ^{145}Gd β decay. The effective blocking by the filled neutron orbitals leaves possible only proton decay transitions to the $\nu s_{1/2}$ level. Only virtual proton pairs from the $\pi s_{1/2}$ or $\pi d_{3/2}$(ℓ-forbidden) can deexcite, in this description, by allowed decay.

Fig. 18 Simplified decay scheme for ^{145}Gd (a) is compared with the decay of the ^{144}Eu core. Note the close agreement between the energy separation and decay intensity pattern of the 2^+ ^{144}Sm core levels and the $(\pi d_{5/2}\times2^+)$ levels in ^{145}Eu. Although the logft's do not compare so well, additional unobserved decay to high energy states in ^{144}Sm can improve that comparison substantially.

Fig. 19 Comparison of the shell+weak-coupling model predicted levels and the experimentally observed levels with logft<7. The single-particle shell-model states at the left are assumed from (p,t) to be identical to the five lowest-lying experimental

levels, the ($\pi d_{5/2}+\otimes 2^+$) energies are taken from the ^{144}Sm core, and the energies of the three-quasiparticle states, coupled to the $\nu f_{1/2}$ and $\nu h_{9/2}$ orbitals, were calculated assuming $\varepsilon_{9/2}-\varepsilon_{11/2}$=5.5 MeV and $V_{9/2\text{-}11/2}$=-1.25 MeV. The calculation of the $\nu f_{7/2}-\nu h_{9/2}$ energy separation (1.4 MeV) agrees closely with that observed in ^{147}Gd so the relative energy of the $\nu i_{13/2}$ coupled state was taken from experiment.

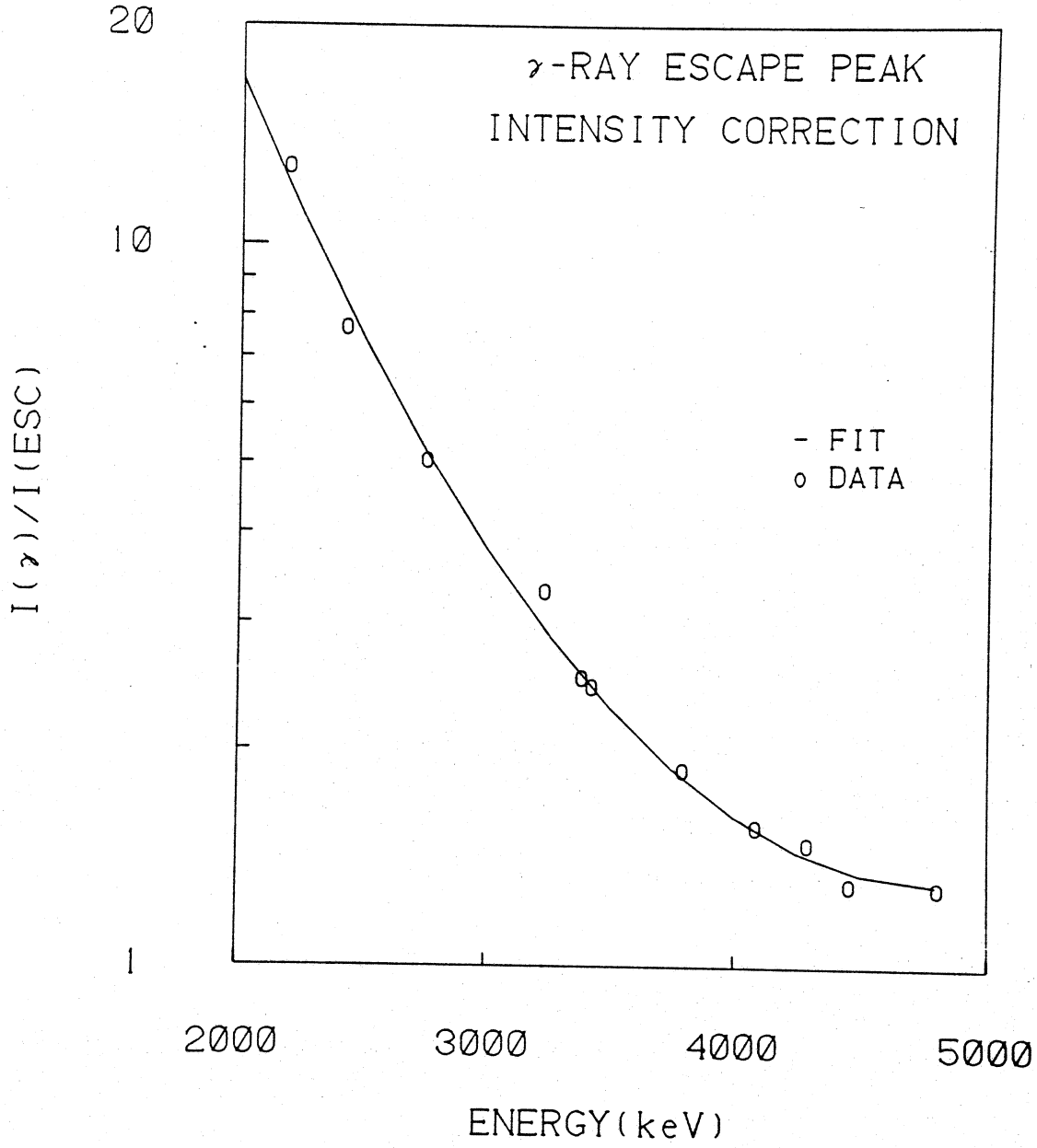
γ-RAY ESCAPE PEAK
INTENSITY CORRECTION
- FIT
o DATA
20
10
1
I(γ)/I(ESC)
2000
3000
4000
5000
ENERGY(keV)
XBL 8012-13604

Figure 1

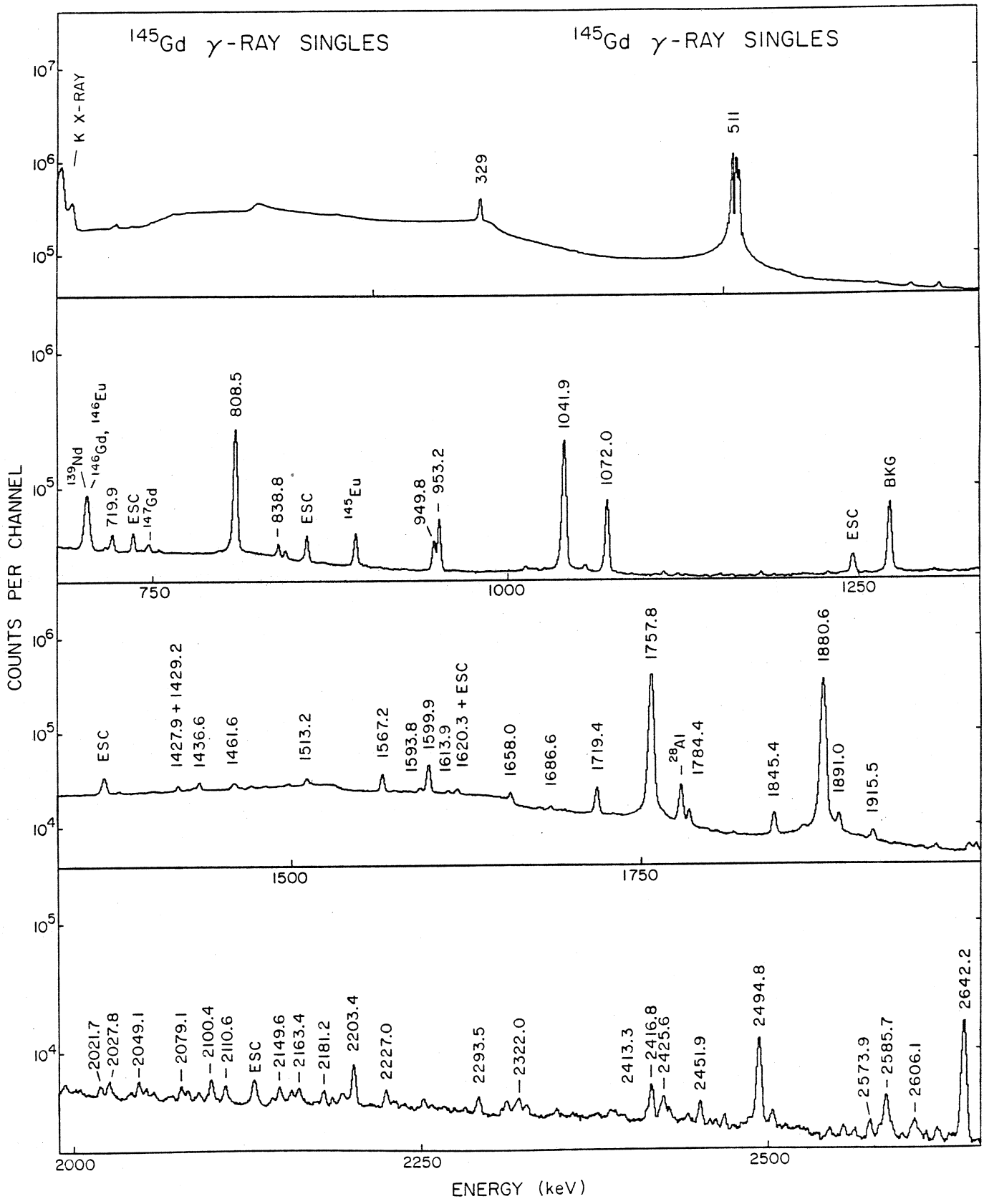
145Gd γ-RAY SINGLES
145Gd γ-RAY SINGLES
K X-RAY
329
511
139Nd
146Gd, 146Eu
719.9
ESC 147Gd
808.5
838.8
ESC
145Eu
949.8
953.2
1041.9
1072.0
ESC
BKG
ESC
1427.9 + 1429.2
1436.6
1461.6
1513.2
1567.2
1593.8
1599.9
1613.9
1620.3 + ESC
1658.0
1686.6
1719.4
1757.8
28Al
1784.4
1845.4
1880.6
1891.0
1915.5
2021.7
2027.8
2049.1
2079.1
2100.4
2110.6
ESC
2149.6
2163.4
2181.2
2203.4
2227.0
2293.5
2322.0
2413.3
2416.8
2425.6
2451.9
2494.8
2573.9
2585.7
2606.1
2642.2
COUNTS PER CHANNEL
ENERGY (keV)

Figure 2

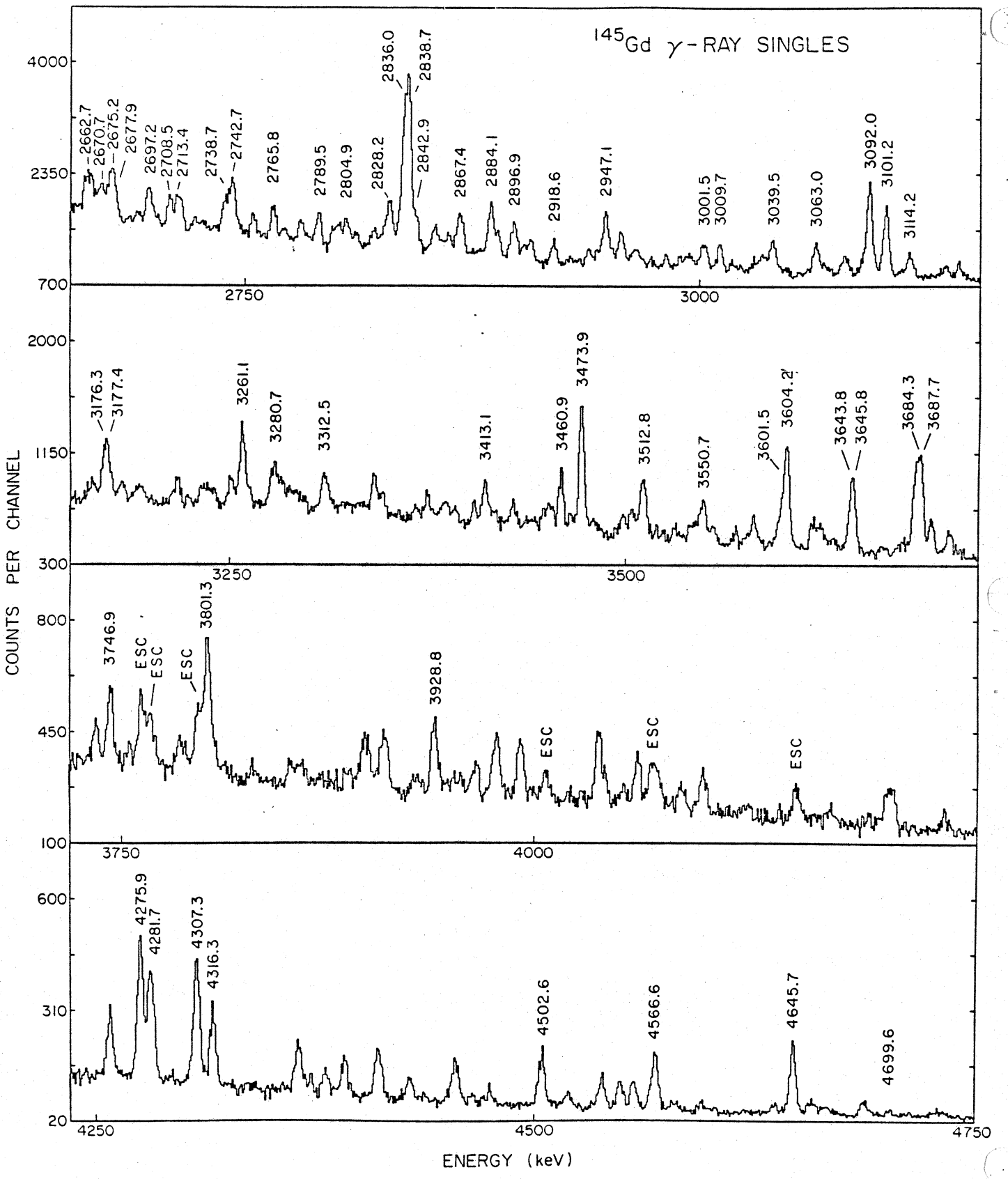

Figure 2 - continued

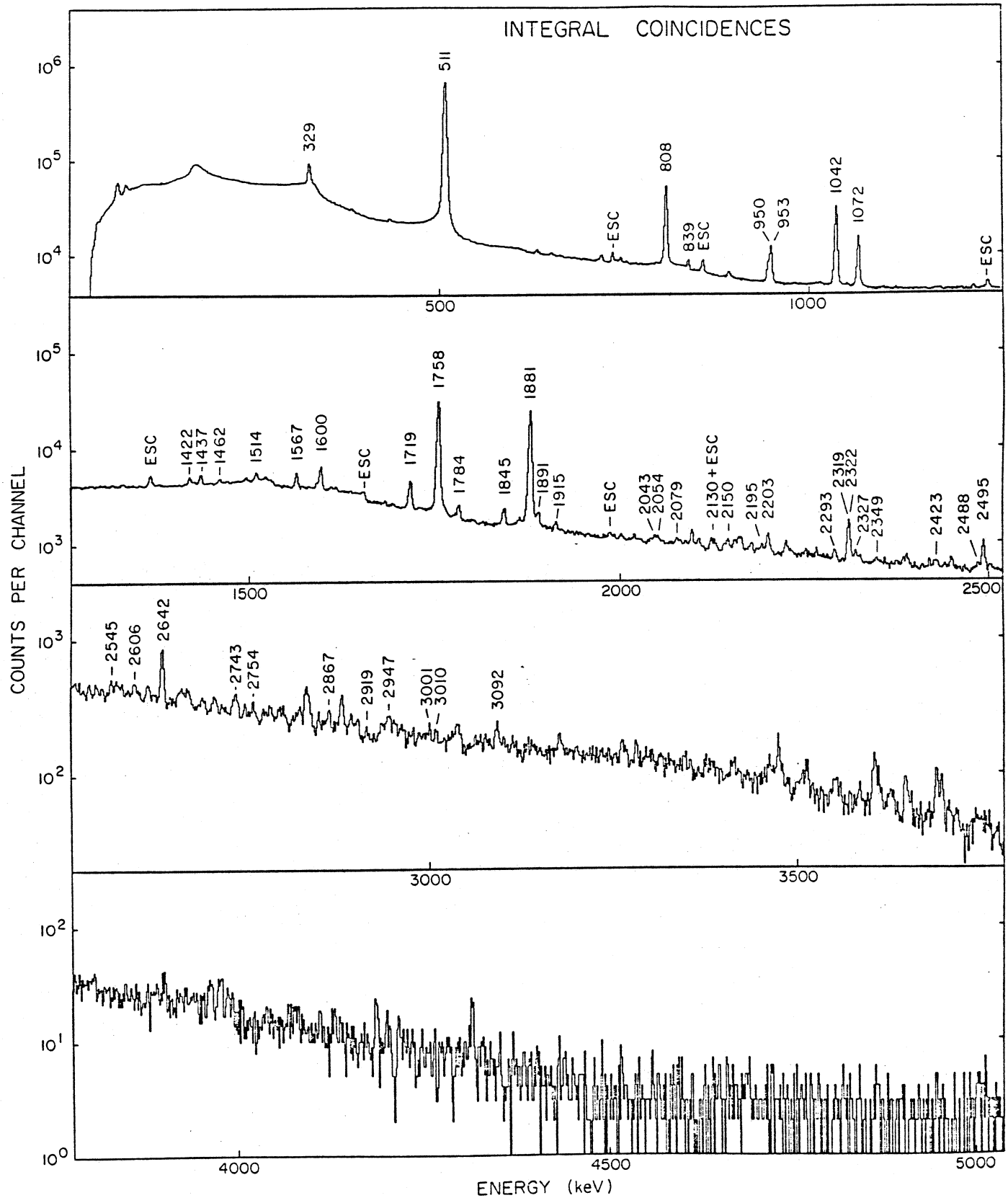
INTEGRAL COINCIDENCES
COUNTS PER CHANNEL
ENERGY (keV)
511
329
808
ESC
839
ESC
950
953
1042
1072
ESC
ESC
1422
1437
1462
1514
1567
1600
ESC
1719
1758
1784
1845
1881
1891
1915
ESC
2043
2054
2079
2130+ESC
2150
2195
2203
2293
2319
2322
2327
2349
2423
2488
2495
2545
2606
2642
2743
2754
2867
2919
2947
3001
3010
3092

figure 3

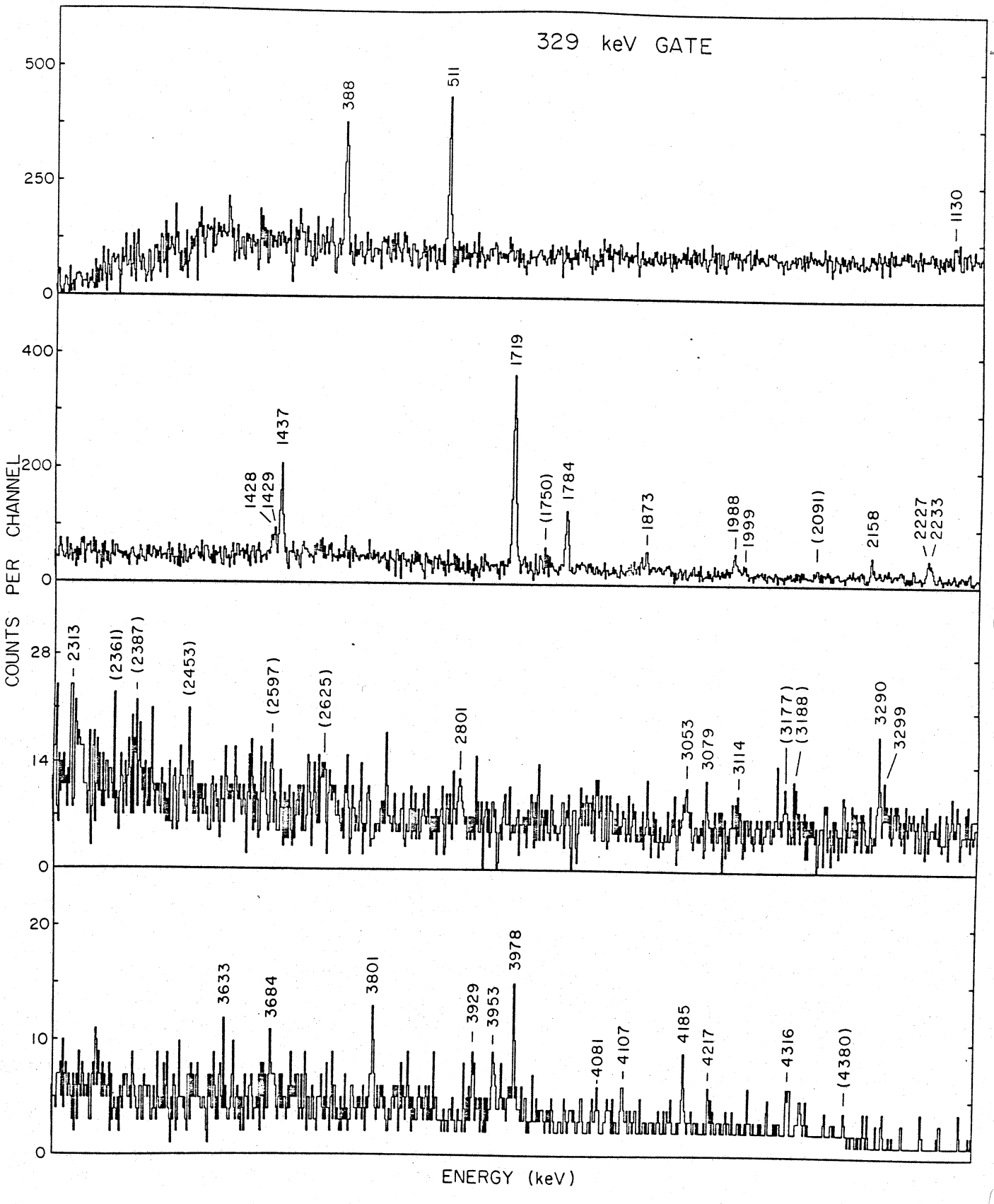
329 keV GATE
388
511
1130
1719
1437
1428
1429
(1750)
1784
1873
1988
1999
(2091)
2158
2227
2233
2313
(2361)
(2387)
(2453)
(2597)
(2625)
2801
3053
3079
3114
(3177)
(3188)
3290
3299
3633
3684
3801
3929
3953
3978
4081
4107
4185
4217
4316
(4380)
500
250
0
400
200
0
28
14
0
20
10
0
COUNTS PER CHANNEL
ENERGY (keV)

figure 4

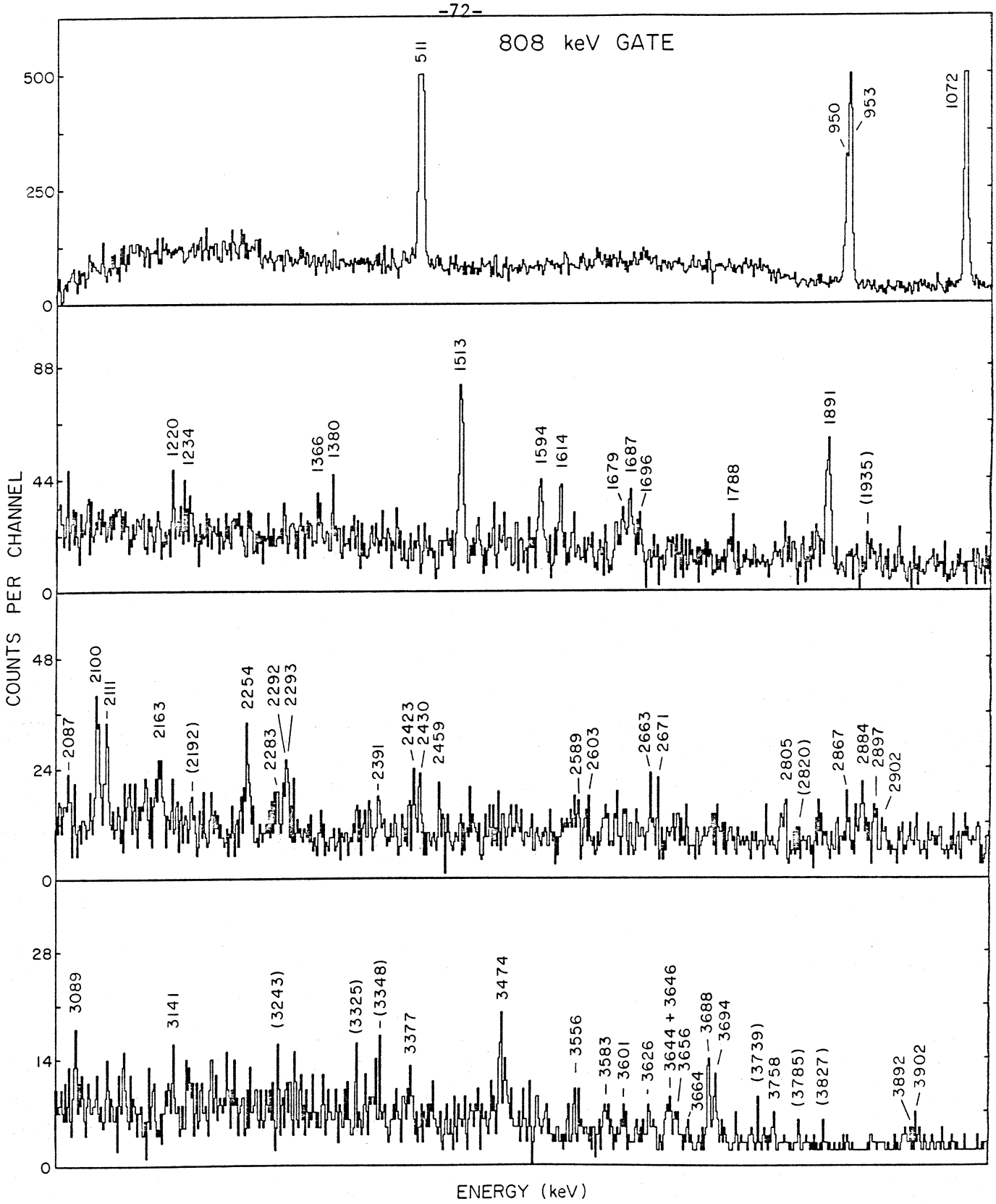
808 keV GATE
511
950
953
1072
1513
1220
1234
1366
1380
1594
1614
1679
1687
1696
1788
1891
(1935)
2087
2100
2111
2163
(2192)
2254
2283
2292
2293
2391
2423
2430
2459
2589
2603
2663
2671
2805
(2820)
2867
2884
2897
2902
3089
3141
(3243)
(3325)
(3348)
3377
3474
3556
3583
3601
3626
3644 + 3646
3656
3664
3688
3694
(3739)
3758
(3785)
(3827)
3892
3902
COUNTS PER CHANNEL
ENERGY (keV)

Figure 5

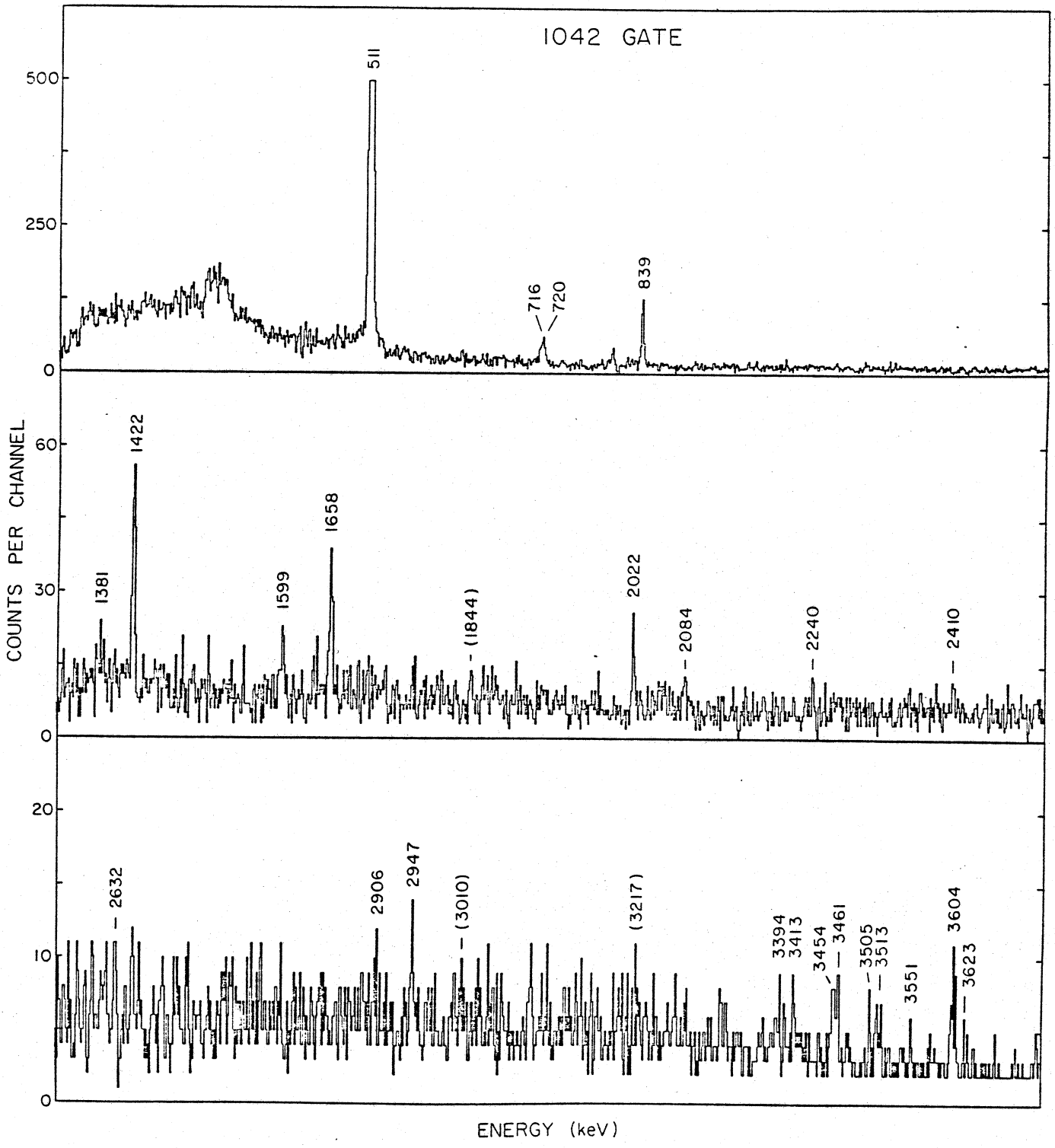
1042 GATE
511
716
720
839
1381
1422
1599
1658
(1844)
2022
2084
2240
2410
2632
2906
2947
(3010)
(3217)
3394
3413
3454
3461
3505
3513
3551
3604
3623
COUNTS PER CHANNEL
ENERGY (keV)

Figure 6

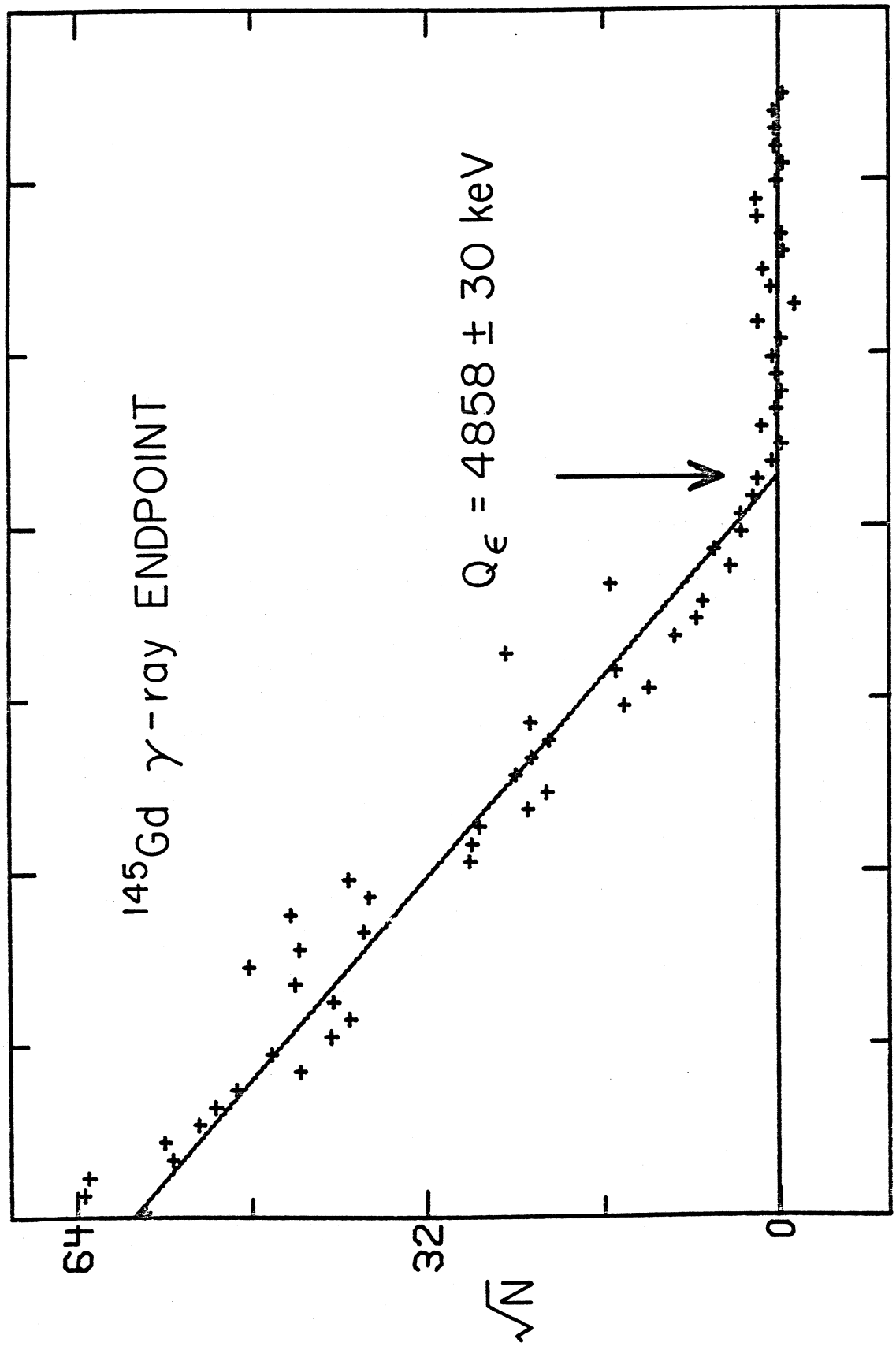
^{145}Gd γ-ray ENDPOINT
Q_ϵ = 4858 ± 30 keV
√N
64
32
0
4000
4400
4800
5200
ENERGY(keV)

Figure 7

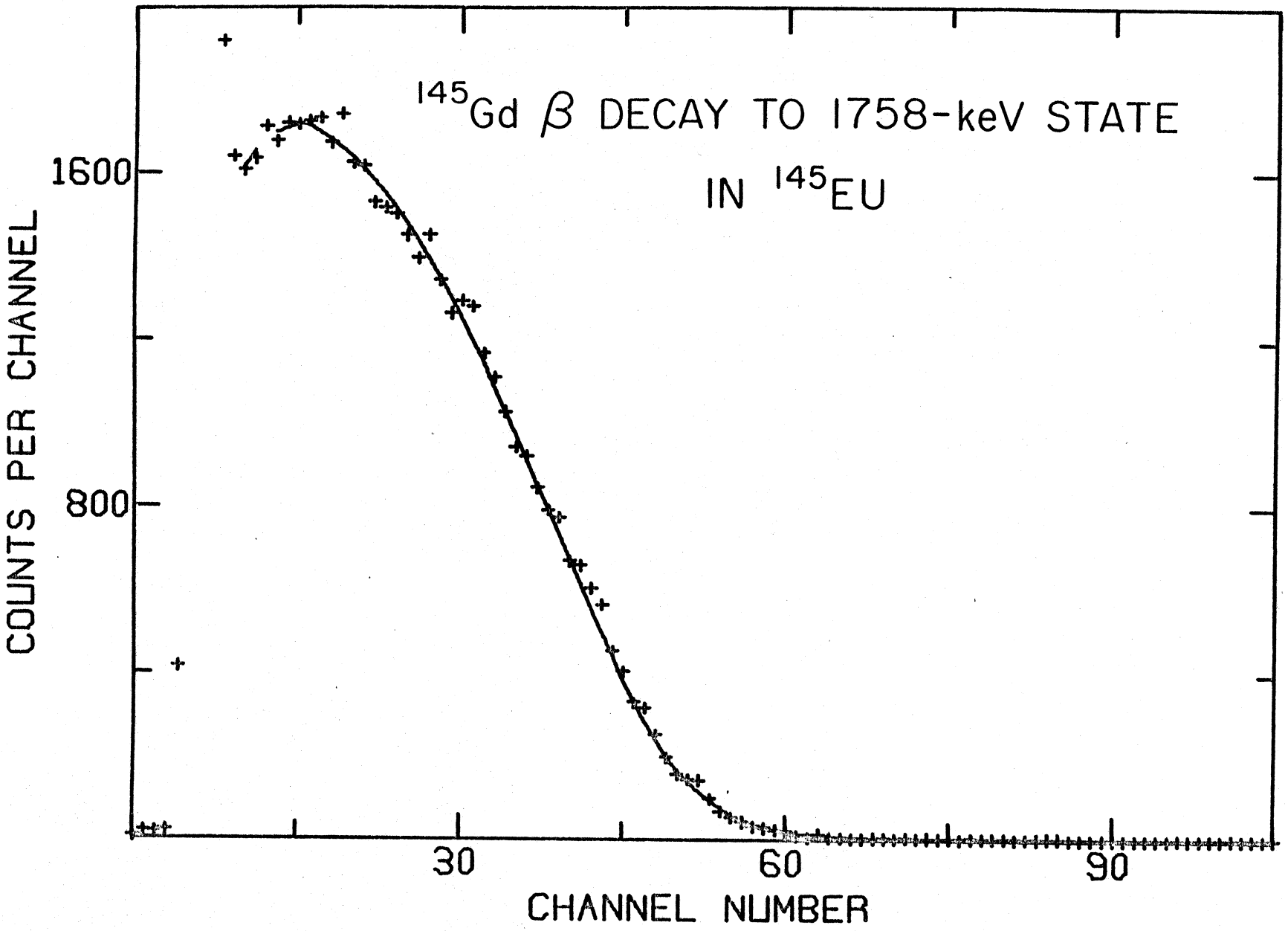
^{145}Gd β DECAY TO 1758-keV STATE
IN ^{145}EU
COUNTS PER CHANNEL
1600
800
30
60
90
CHANNEL NUMBER

Figure 8

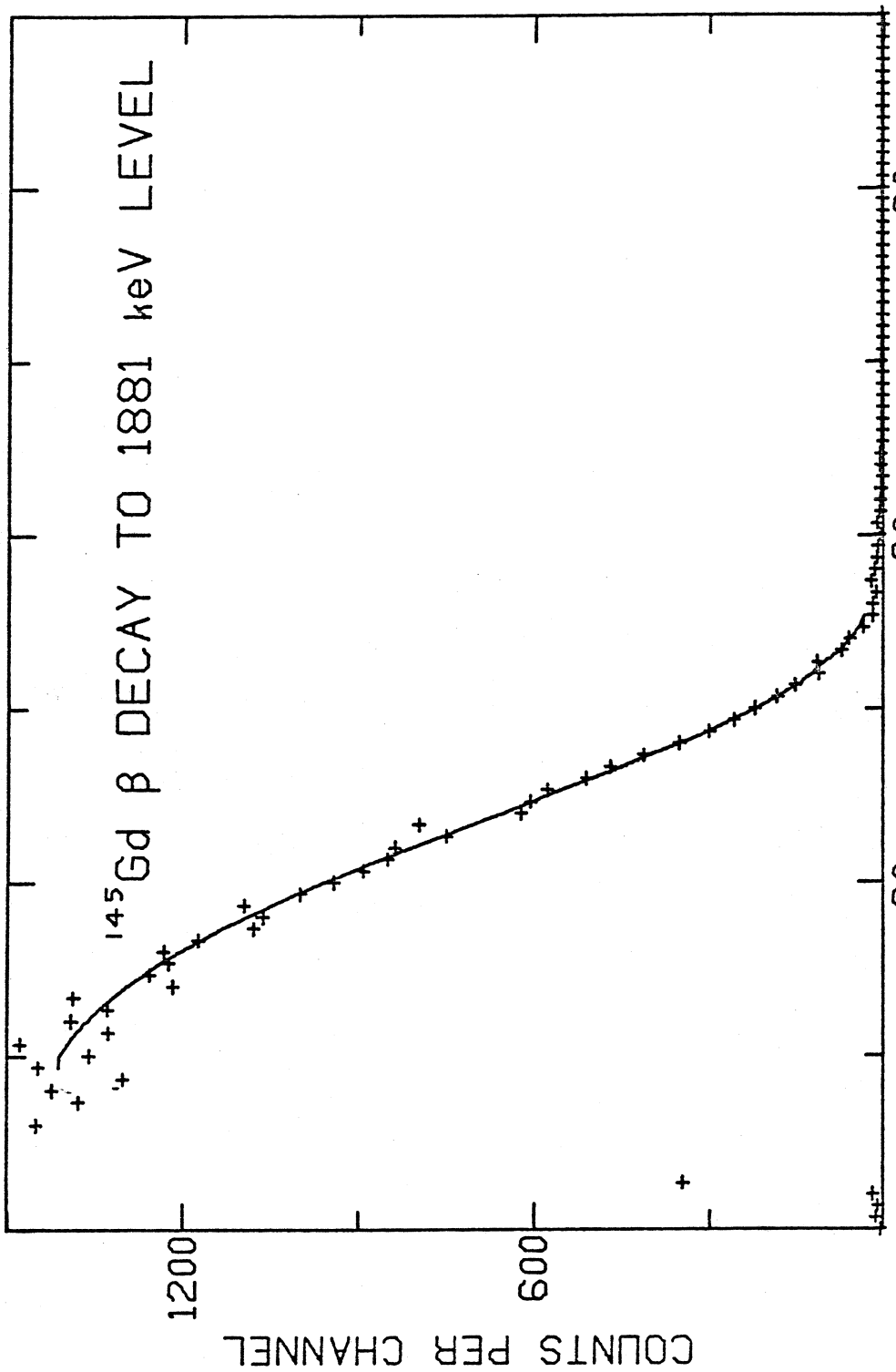

XBL 813-8492

Figure 9

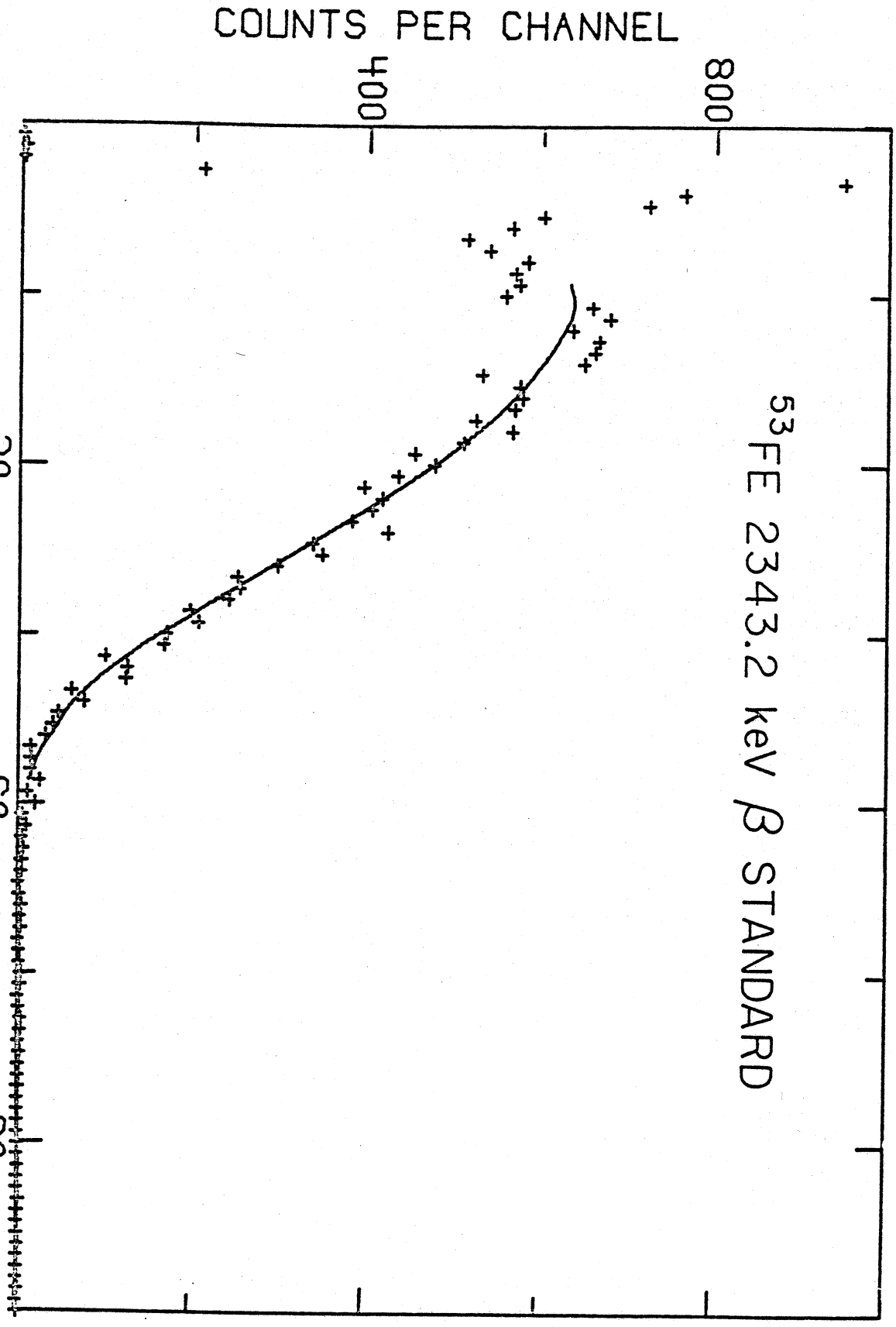
COUNTS PER CHANNEL
400
800
30
60
90
CHANNEL NUMBER
^{53}FE 2343.2 keV β STANDARD

Figure 10

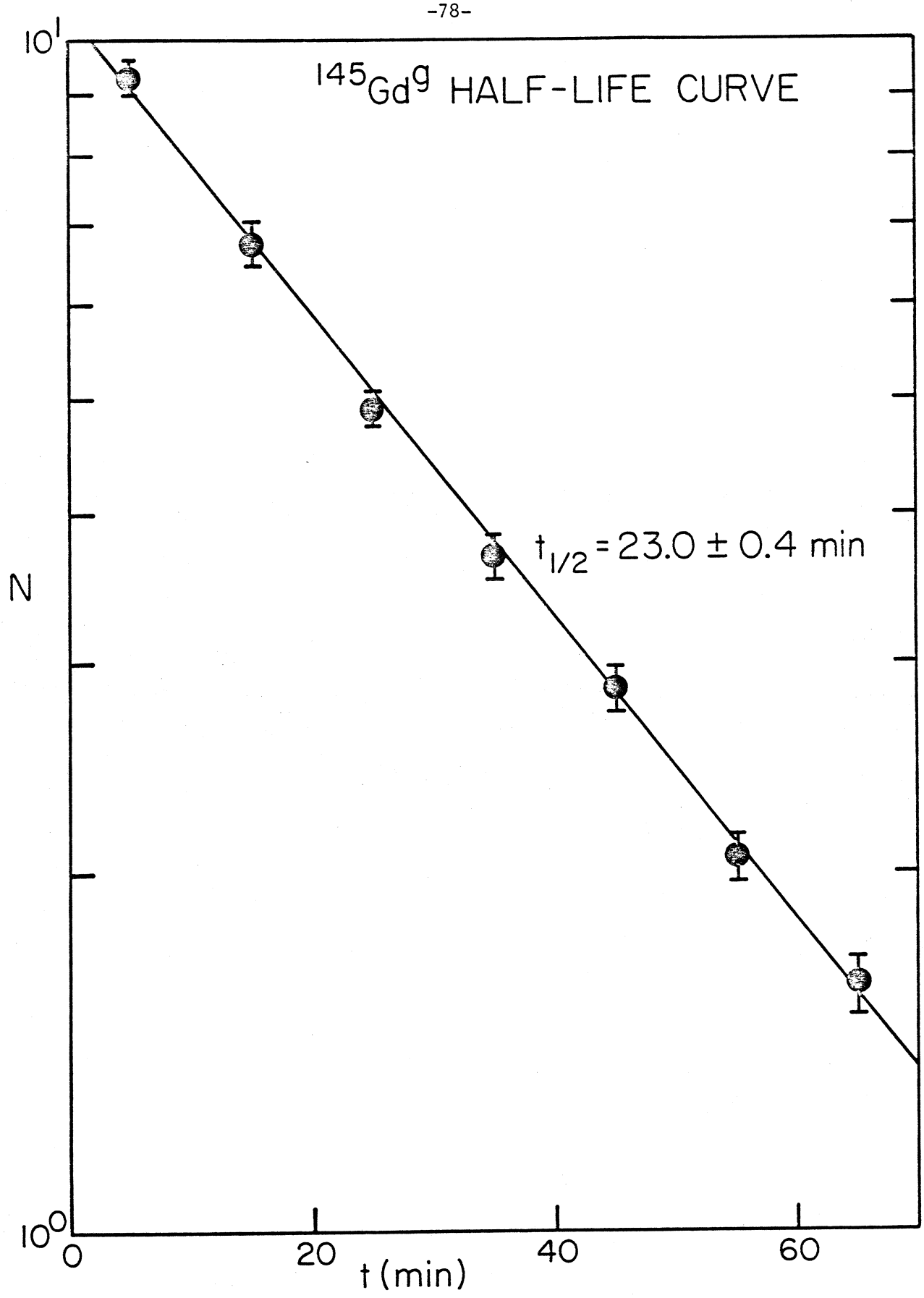
$^{145}Gd^{g}$ HALF-LIFE CURVE
$t_{1/2} = 23.0 \pm 0.4$ min
N
10^1
10^0
0
20
40
60
t (min)

Figure 11

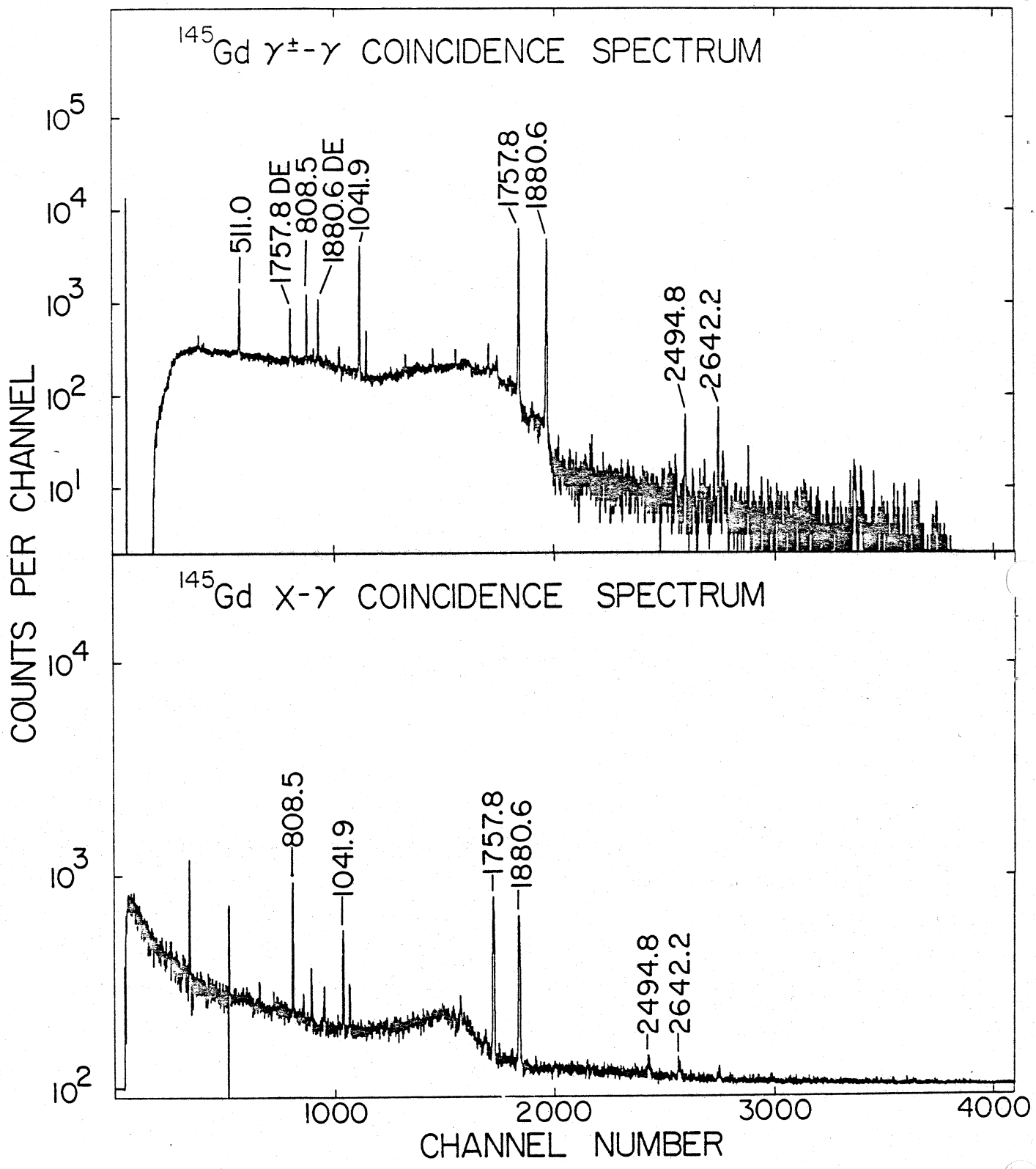
^{145}Gd $\gamma^{\pm}$-γ COINCIDENCE SPECTRUM
511.0
1757.8 DE
808.5
1880.6 DE
1041.9
1757.8
1880.6
2494.8
2642.2
^{145}Gd X-γ COINCIDENCE SPECTRUM
808.5
1041.9
1757.8
1880.6
2494.8
2642.2
COUNTS PER CHANNEL
CHANNEL NUMBER
1000
2000
3000
4000

Figure 12

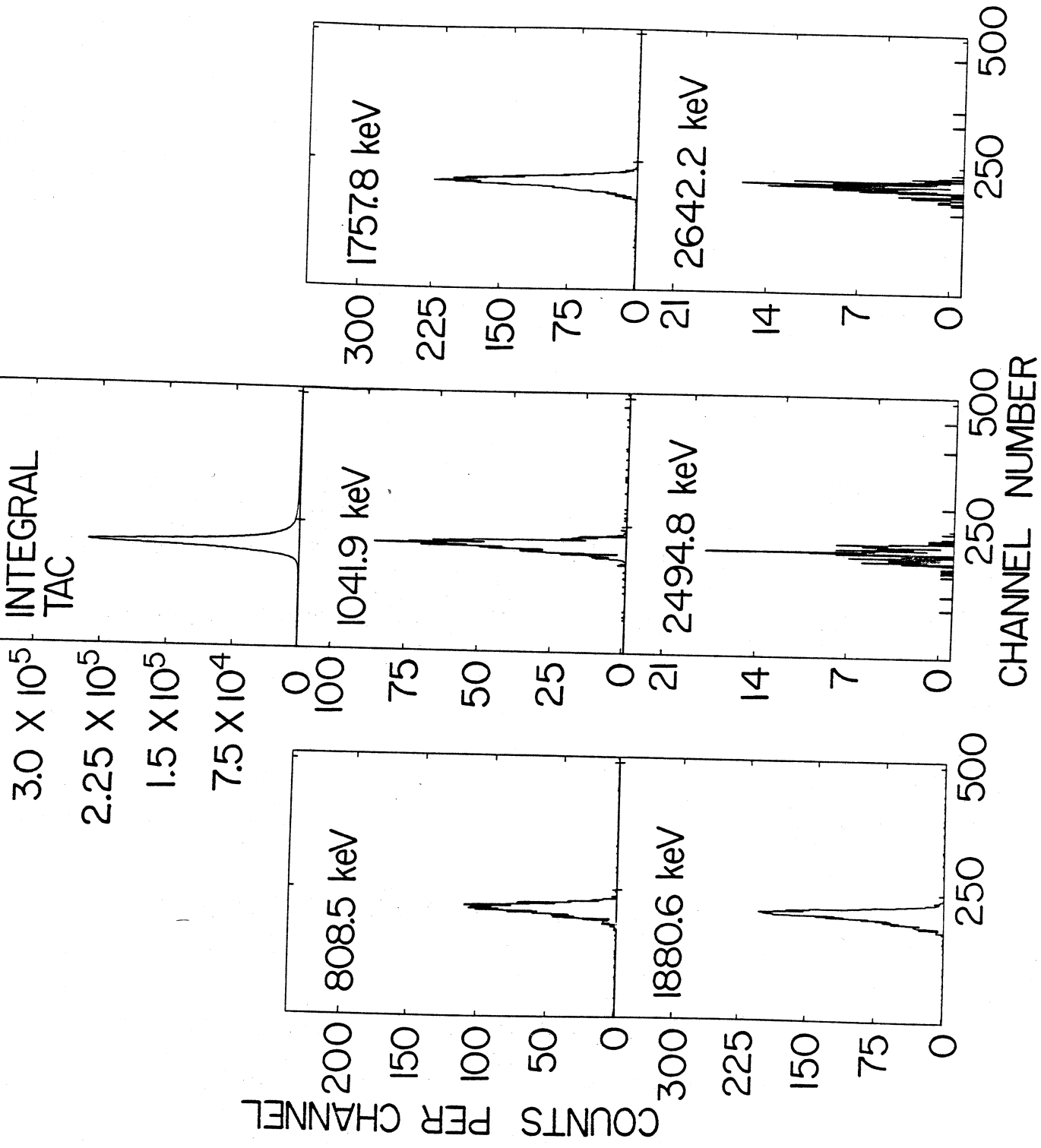
INTEGRAL TAC
1041.9 keV
2494.8 keV
808.5 keV
1880.6 keV
17578 keV
2642.2 keV
COUNTS PER CHANNEL
CHANNEL NUMBER

Figure 13

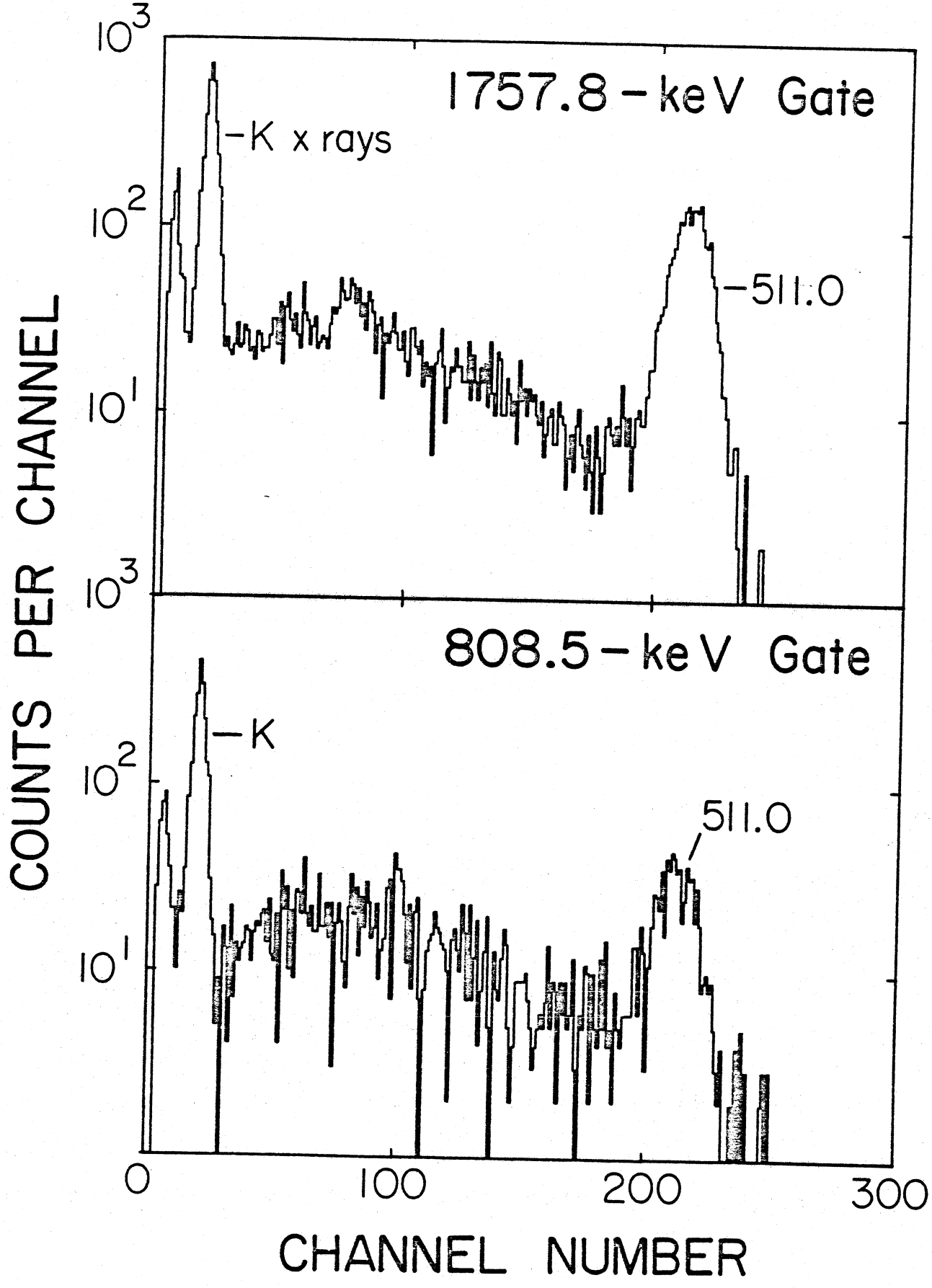
1757.8 - keV Gate
K x rays
511.0
808.5 - keV Gate
K
511.0
COUNTS PER CHANNEL
CHANNEL NUMBER
10^3
10^2
10^1
0
100
200
300

Figure 14

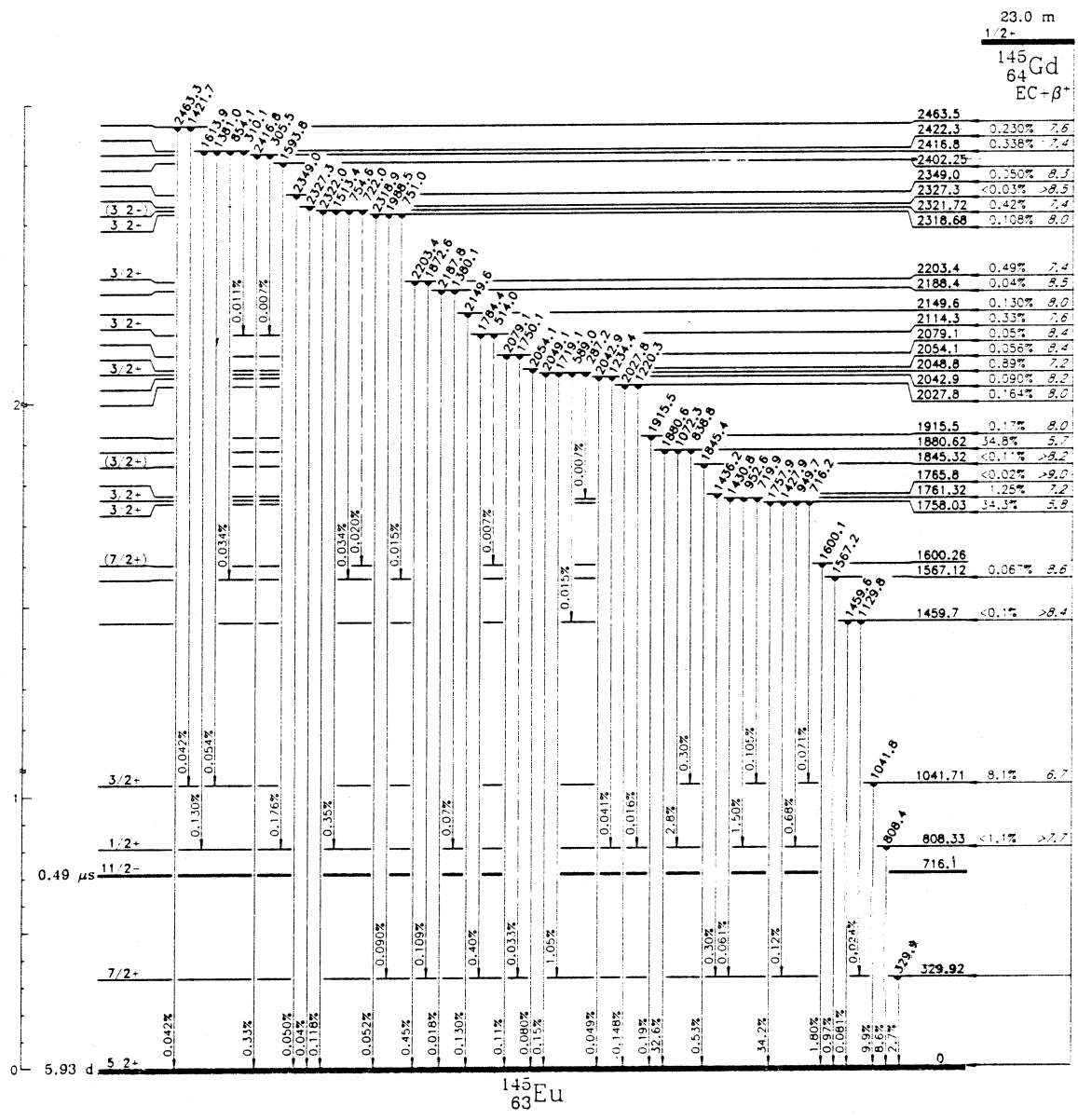
23.0 m
1/2+
145 64 Gd
EC+β+
2463.5
2422.3 0.230% 7.6
2416.8 0.338% 7.4
2402.25
2349.0 0.350% 8.3
2327.3 <0.03% >8.5
2321.72 0.42% 7.4
2318.68 0.108% 8.0
2203.4 0.49% 7.4
2188.4 0.04% 8.5
2149.6 0.130% 8.0
2114.3 0.33% 7.6
2079.1 0.05% 8.4
2054.1 0.056% 8.4
2048.8 0.89% 7.2
2042.9 0.090% 8.2
2027.8 0.164% 8.0
1915.5 0.17% 8.0
1880.62 34.8% 5.7
1845.32 <0.11% >8.2
1765.8 <0.02% >9.0
1761.32 1.25% 7.2
1758.03 34.3% 5.9
1600.26
1567.12 0.067% 8.6
1459.7 <0.1% >8.4
1041.71 8.1% 6.7
808.33 <1.1% >7.7
716.1
329.92
0.49 μs
5.93 d
145 63 Eu
XBL 813-8491

Figure 15

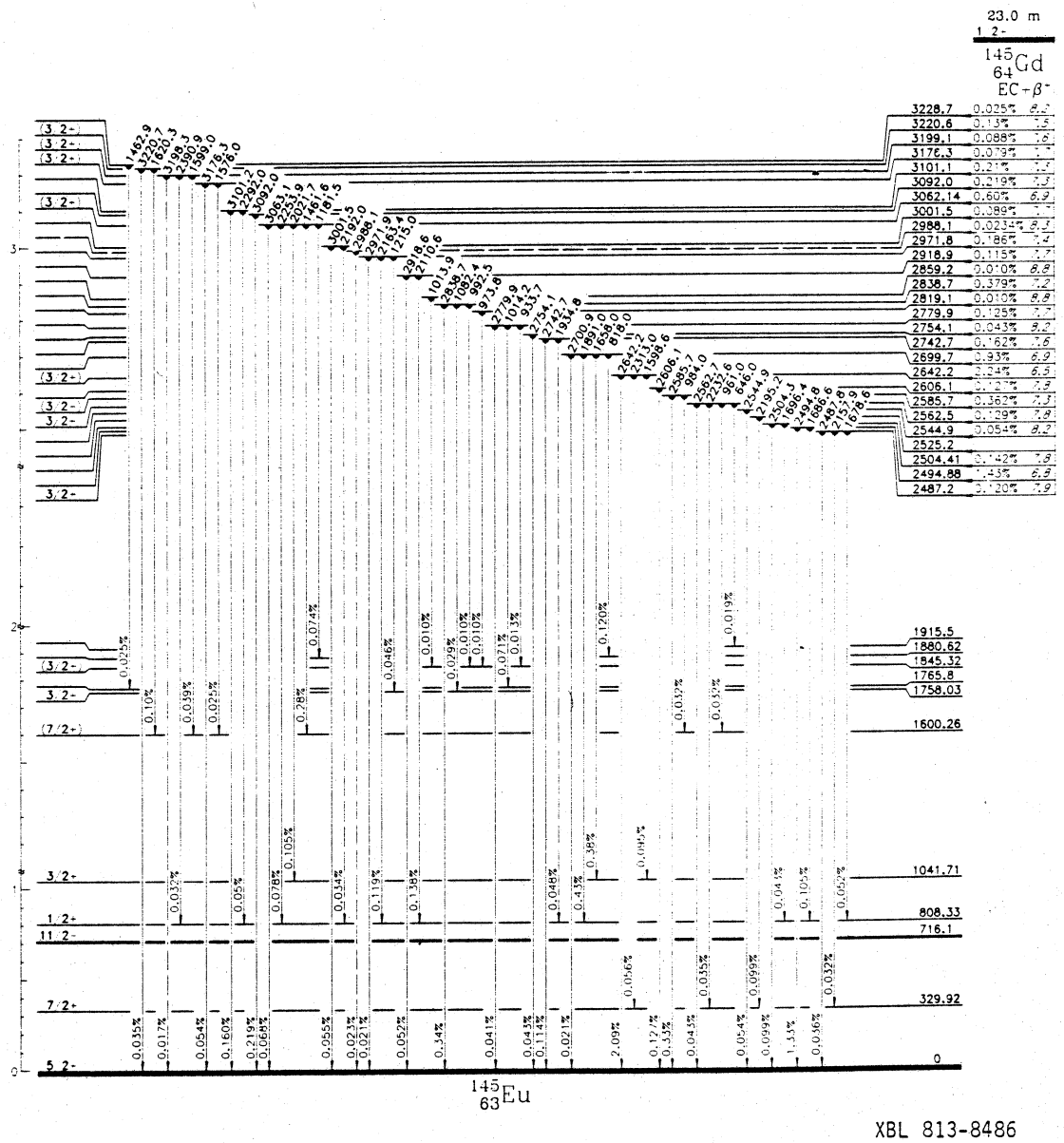

Figure 15 - continued (2)

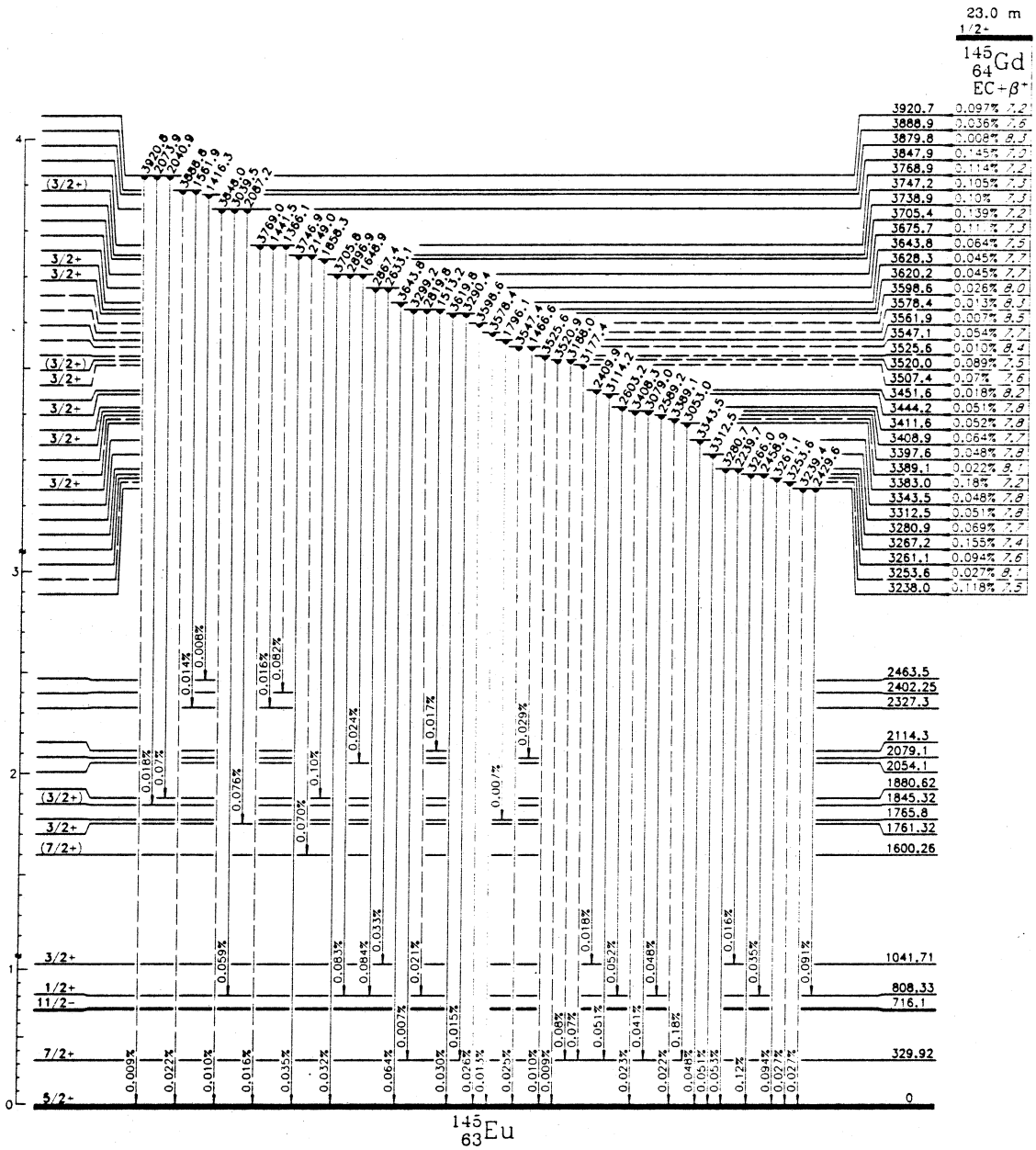

Figure 15 - continued (3)

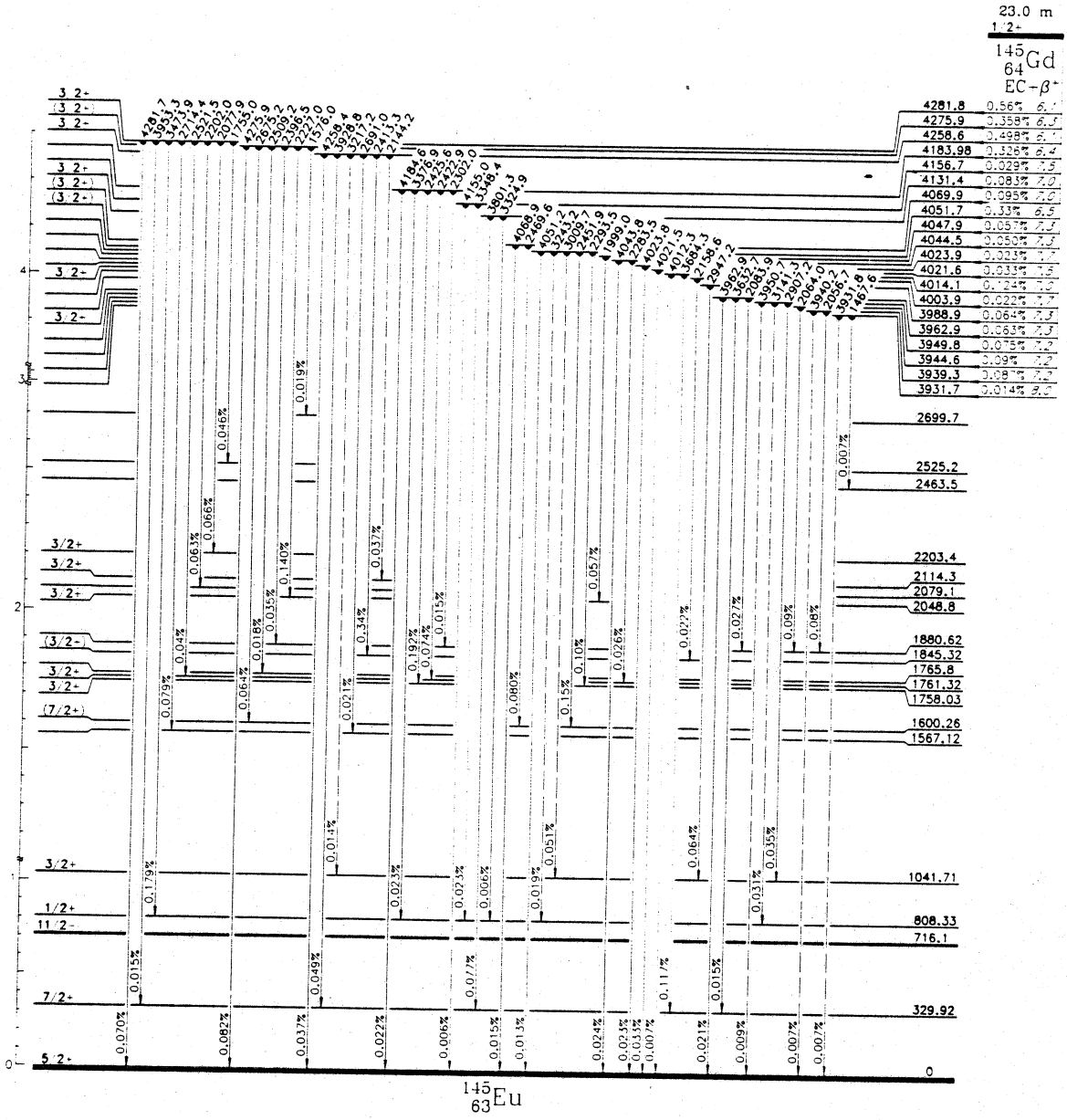

XBL 813-8488

Figure 15 - continued (4)

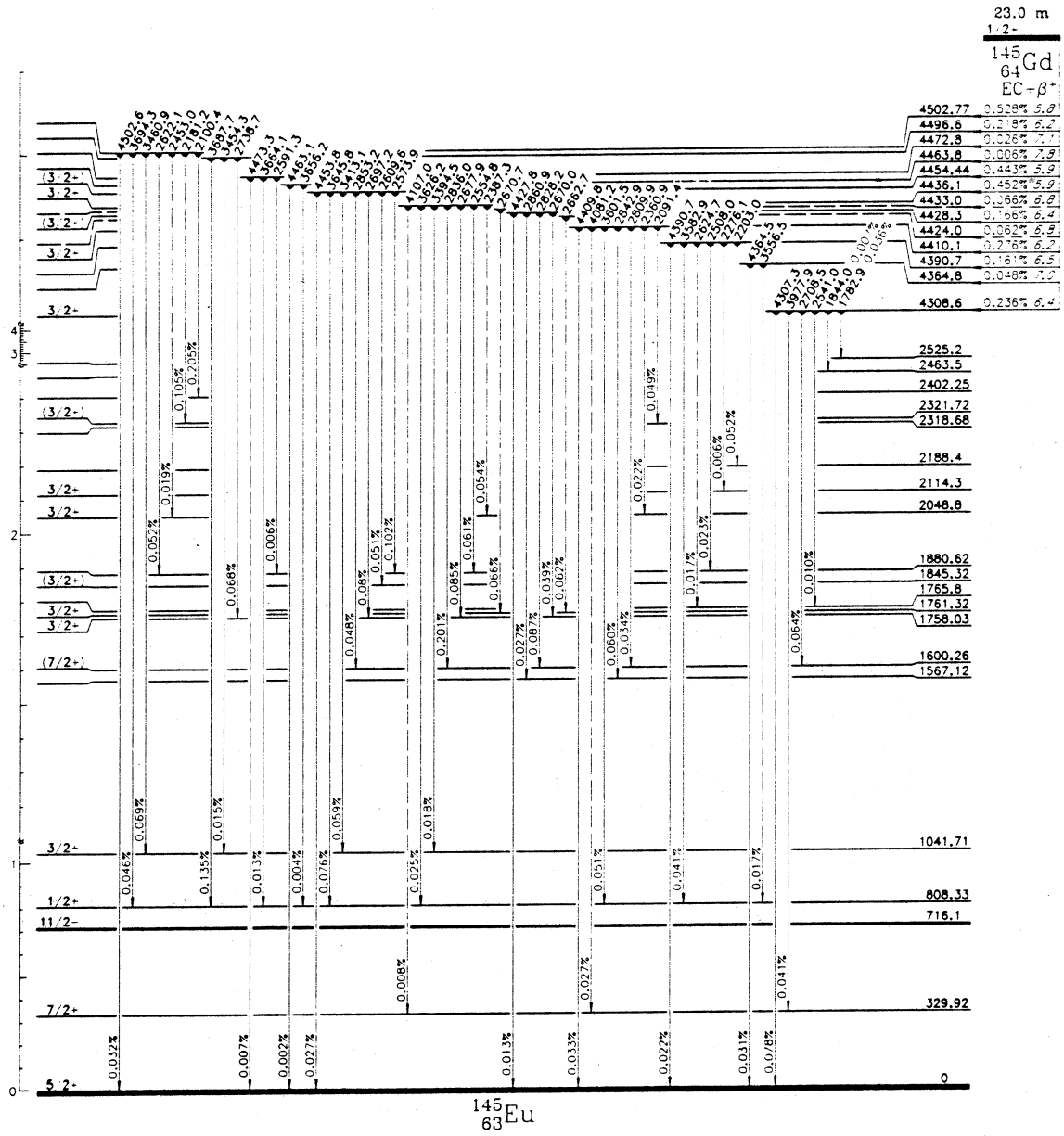

XBL 813-8489

Figure 15 - continued (5)

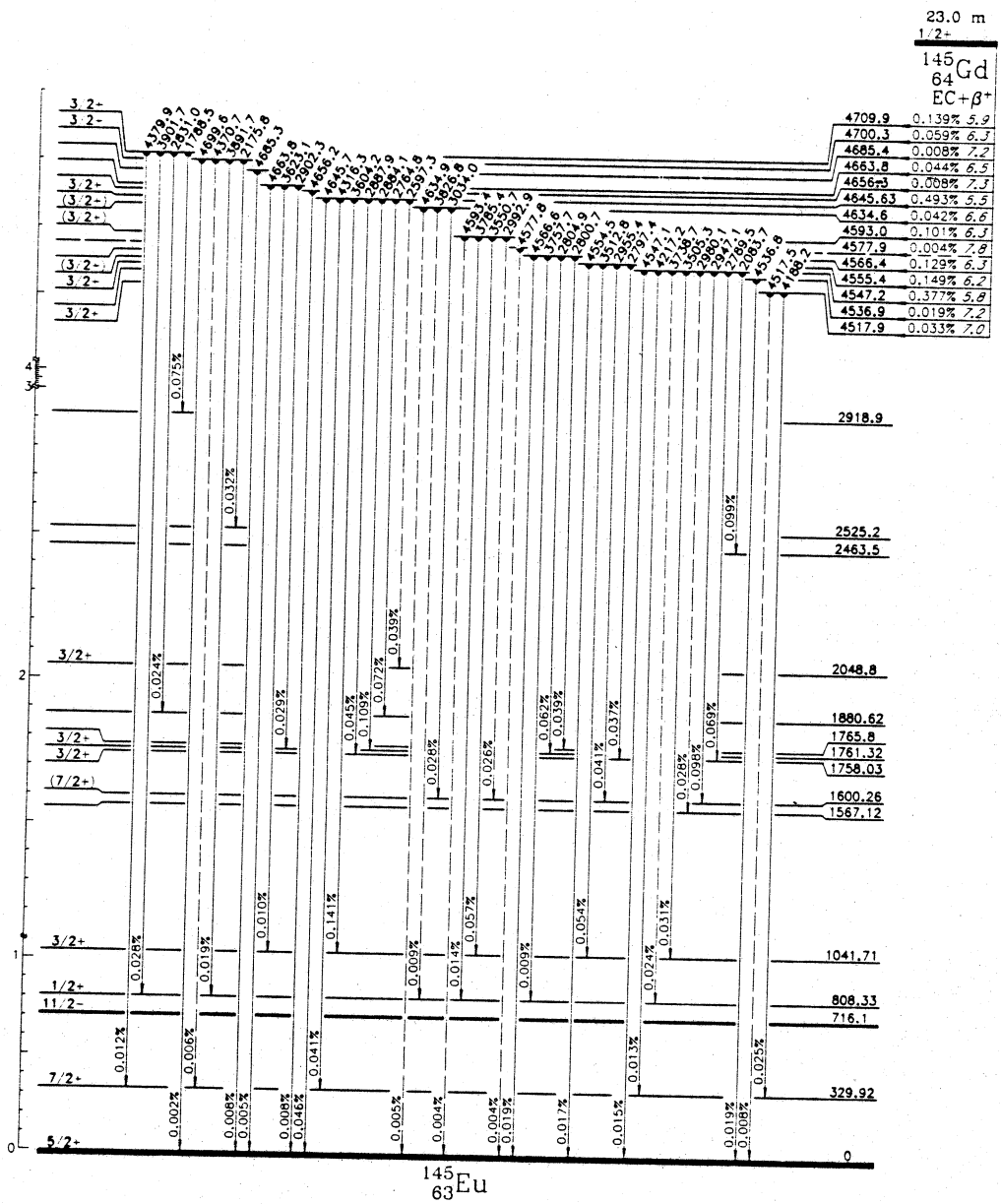

Figure 15 - continued (6)

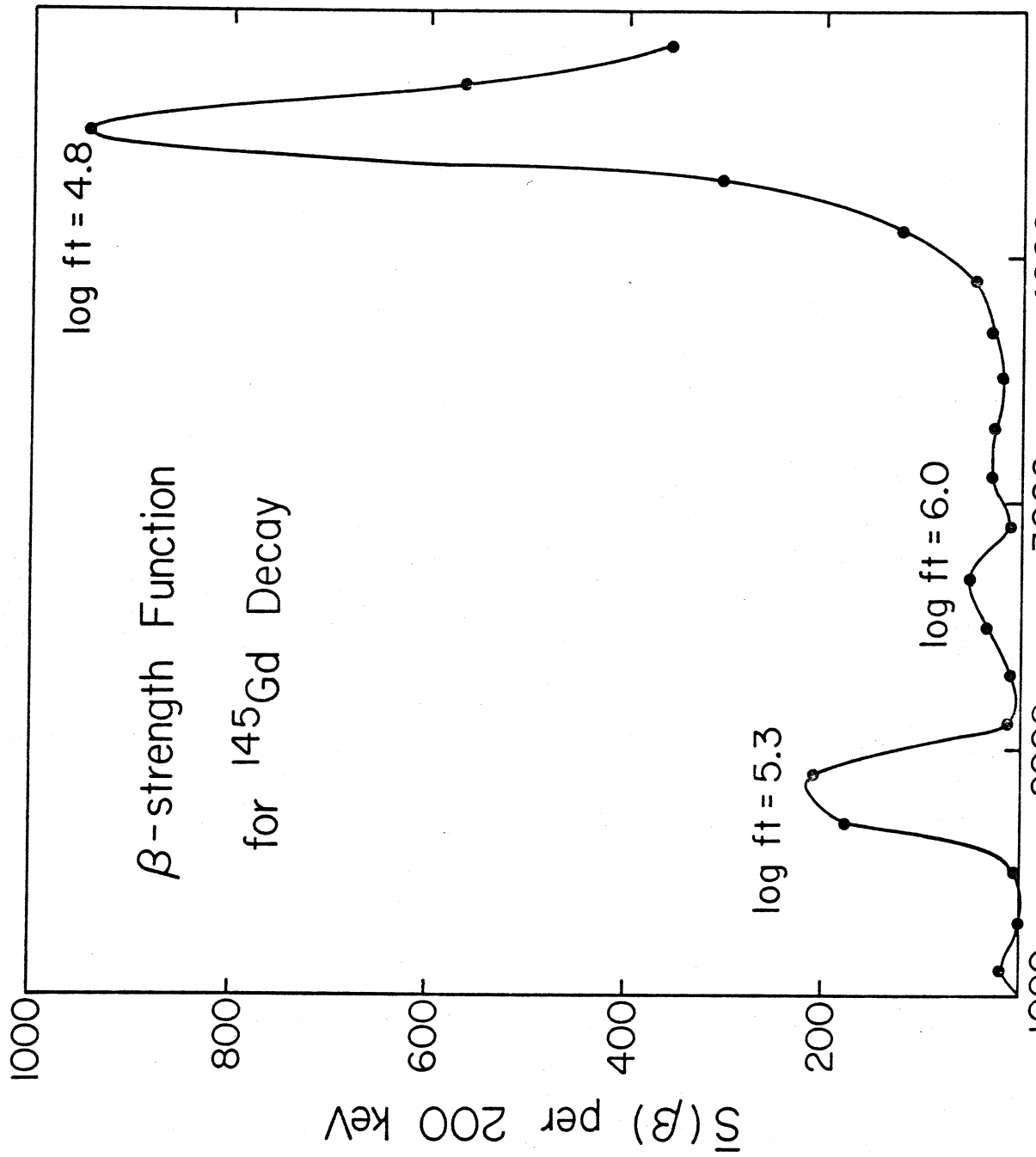
β-strength Function
for ^{145}Gd Decay
log ft = 4.8
log ft = 5.3
log ft = 6.0
S(β) per 200 keV
Excitation Energy in ^{145}Eu (keV)
1000
800
600
400
200
1000
2000
3000
4000

Figure 16

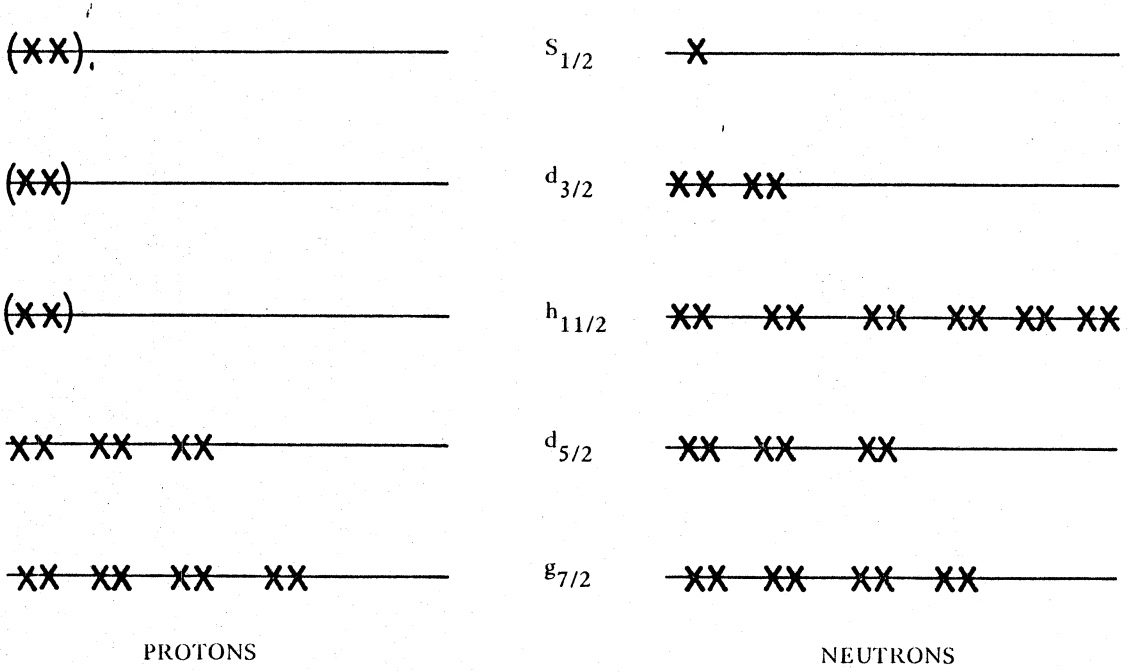

$^{145}_{64}Gd_{81}$

XBL 811-124

Figure 17

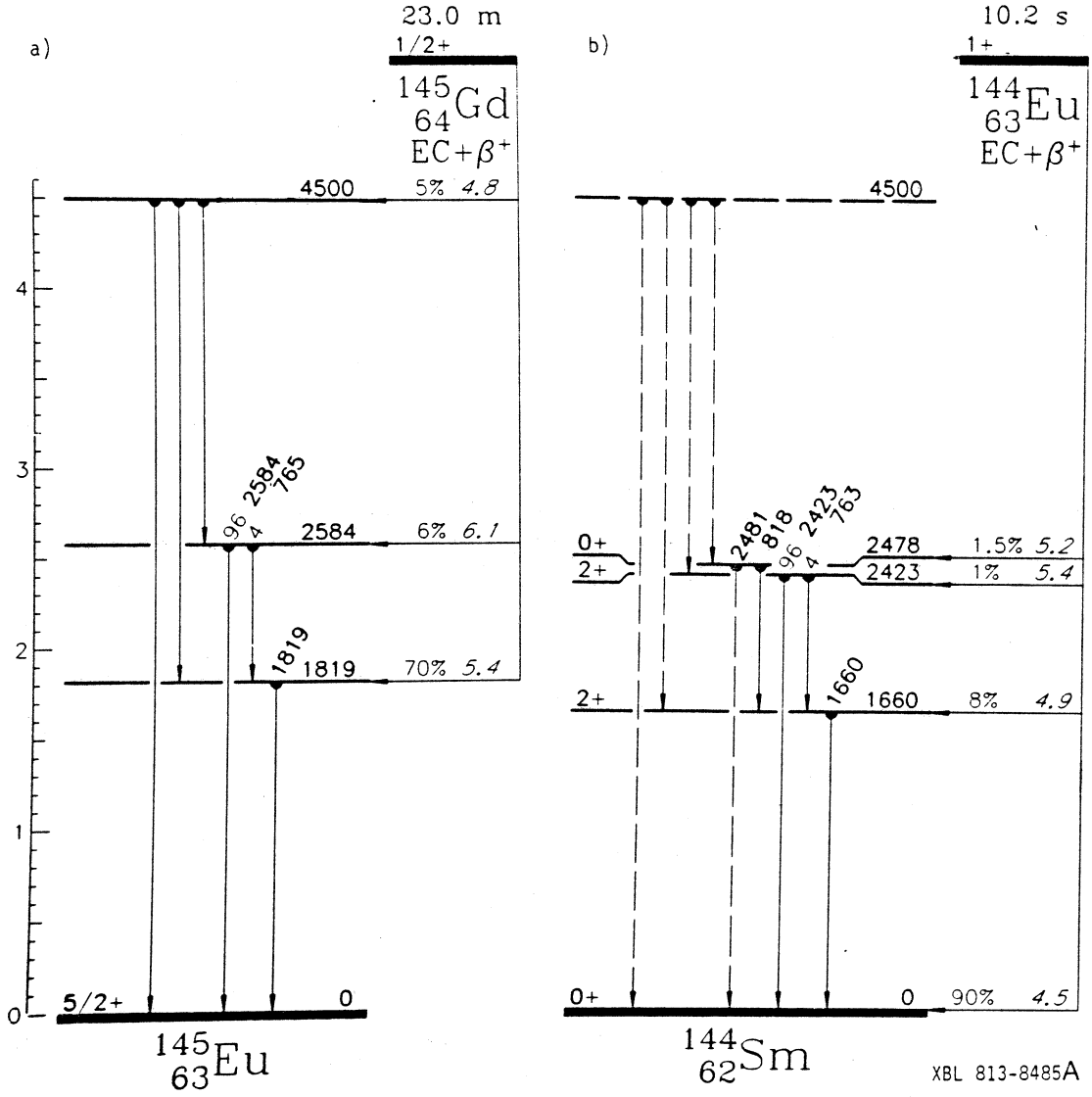
a)
23.0 m
1/2+
145 64 Gd
EC+β+
4500
5% 4.8
2584
6% 6.1
1819
70% 5.4
0
5/2+
145 63 Eu
b)
10.2 s
1+
144 63 Eu
EC+β+
4500
0+
2+
2478
1.5% 5.2
2423
1%
5.4
2+
1660
8%
4.9
0+
0
90%
4.5
144 62 Sm
XBL 813-8485A

Figure 18

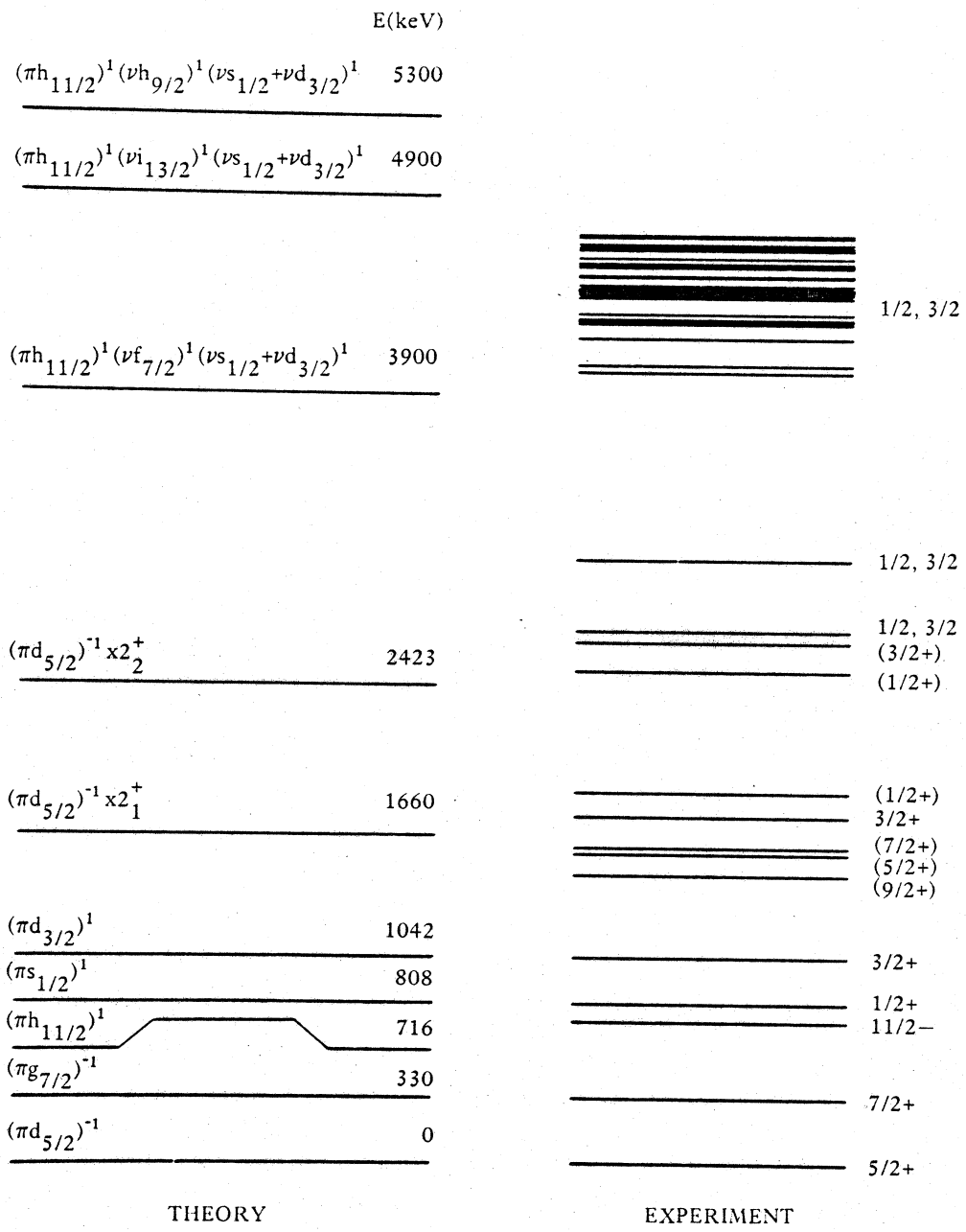

$^{145}_{63}Eu$

-- XBL 8012-13602

Figure 19